Chemical Engineering Journal 412 (2021) 128637

Contents lists available at ScienceDirect

Chemical Engineering Journal

journal homepage: www.elsevier.com/locate/cej

Synthesis and application of Zn-doped polyaniline modified multi-walled carbon nanotubes as stimuli-responsive nanocarrier in the epoxy matrix for achieving excellent barrier-self-healing corrosion protection potency

Parisa Najmi [a,b,1], Navid Keshmiri [a,b,1], Mohammad Ramezanzadeh [a], Bahram Ramezanzadeh [a,*]

[a] Surface Coating and Corrosion Department, Institute for Color Science and Technology, Tehran, Iran
[b] Polymer Engineering Department, Amirkabir University of Technology, Tehran, Iran

ARTICLE INFO

Keywords:
Multi-walled carbon nanotube
Polyaniline
Self-healing
Epoxy
Nano-composite coating

ABSTRACT

Multi-walled carbon nanotubes (MWCNTs), which are one of the most favorable large aspect ratio hollow-cylindrical nanomaterials, have been considered for numerous advanced applications due to their exceptional thermal-mechanical and electrical characteristics. However, because of the high surface area and being susceptible to agglomeration, they suffered from low dispersion ability. Thus, functionalization with organic and inorganic materials is one of the promising solutions to their limitations. Due to the presence of sp^2-bonded carbon atoms, they have no functionalities. One way to generate carboxylic functionalities on MWCNTs is their oxidation. Herein, this study reports the synthesis of a novel highly-oxidized multi-walled carbon nanotube (O-MWCNT) particles modified by the polyaniline (PANI) nanofibers and their performance in the epoxy-based nanocomposites for achieving passive/active anti-corrosion system with efficacious self-healing potency and barrier anti-corrosion characteristic. The O-MWCNT-PANI nanocomposite was then modified by the zinc metal cations to accomplish a smart self-healing anti-corrosion system. The total resistance of about 4000 ohm.cm^2 was achieved in the extract with O-MWCNT-PANI-Zn, while the blank sample showed a resistance of about 1200 ohm.cm^2 after three hours of immersion time. The most noticeable enhancement of the dual active-barrier protection was obtained in the scratched coatings with modified nano-inhibitors. The more $log|Z|_{10\ mHz}$ values were reached, including 4.82 ohm.cm^2 and 5.06 ohm.cm^2, in O-MWCNT-PANI/EP and O-MWCNT-PANI-Zn/EP, respectively.

1. Introduction

The epoxy (EP) coatings are among the most favorable polymeric coatings applied on the metal substrates to enhance the anti-corrosion function besides the other features, including good adhesion, high thermal and mechanical stability, and low cost [1]. However, the aggressive conditions and long-term exposure of the EP coatings can significantly affect their corrosion protection durability by diffusion of aggressive ions (Cl^-) into the coatings' porosities and cavities [2,3]. Furthermore, their insufficient crack resistance has led the researchers to improve their properties in different ways [4]. Using conventional anti-corrosive pigments in the polymeric matrix is one of the most promising solutions used to enhance the corrosion resistance [5], physicochemical, and adhesion properties of the organic coatings [5–12]. However, some of these systems provide limited and short-term anti-corrosion performance with a lack of self-healing potency. Achieving long-term protective systems with good anti-corrosion durability requires self-healing materials released at the cathodic and the anodic points in demand. Capsules-based materials [13,14], double-layer hydroxides [15,16], halloysites [17], nano mesoporous silica [18,19], and the most state of the art, graphene oxide [20], are among the important micro/nanocontainers. Loading the organic/inorganic inhibitors in the nanocontainers results in the inhibitors' release in a long time, enhancing the system's corrosion protection activity during the exposure time [21,22].

Newly, carbon-based nanomaterials, like graphene oxide (GO) [23] and CNT [24], have been successfully applied as anti-corrosive materials in polymer composites. The two-dimensional sheet-like structure of GO

* Corresponding author.
E-mail addresses: ramezanzadeh@aut.ac.ir, ramezanzadeh-bh@icrc.ac.ir (B. Ramezanzadeh).
[1] Parisa Najmi and Navid Keshmiri contributed equally to this work.

https://doi.org/10.1016/j.cej.2021.128637
Received 13 October 2020; Received in revised form 5 December 2020; Accepted 18 January 2021
Available online 23 January 2021
1385-8947/

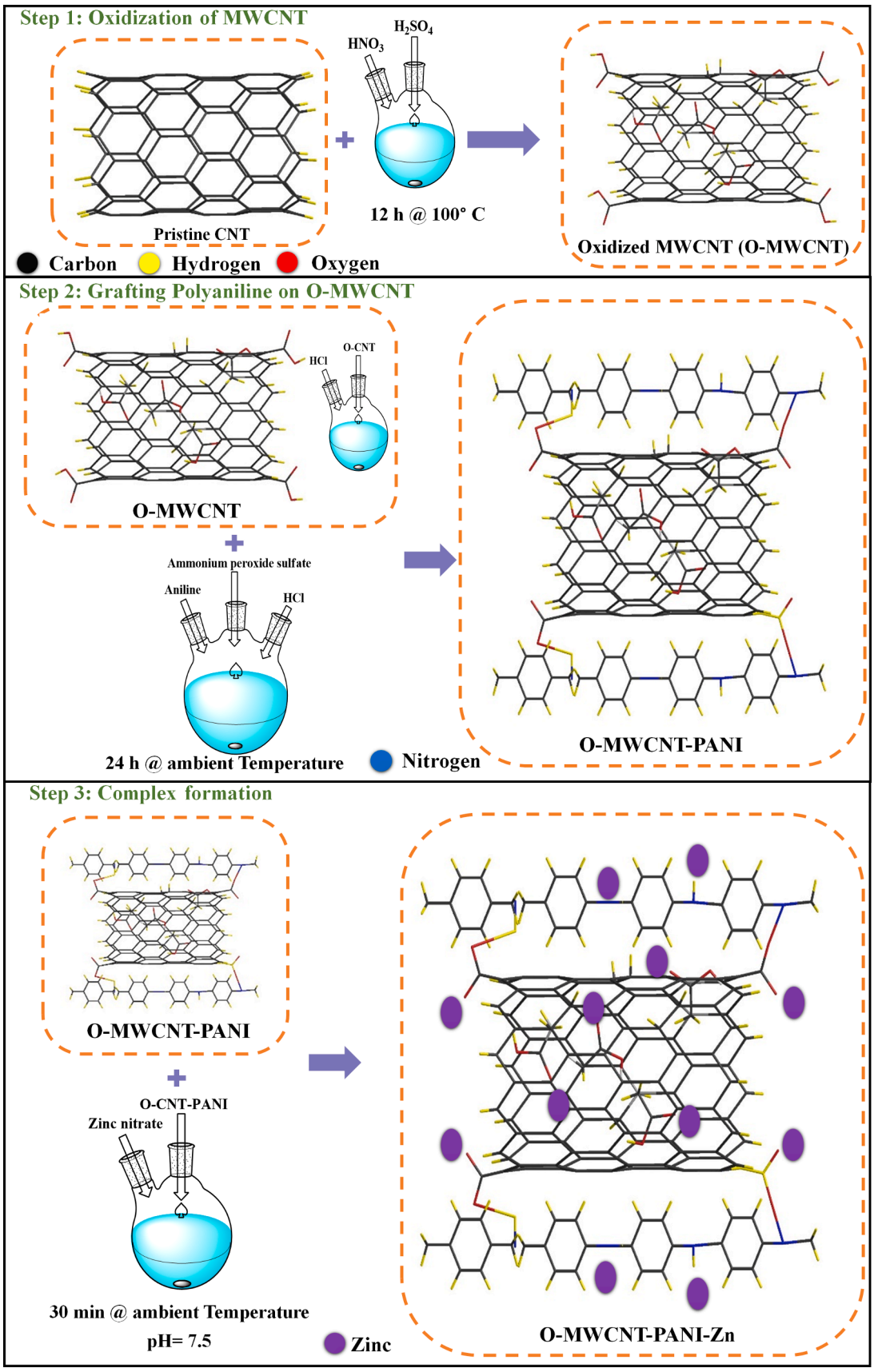

Fig. 1. Illustration of synthesis procedure of O-MWCNT, O-MWCNT-PANI and O-MWCNT-PANI-Zn carbon-based nano materials.

has resulted in rising the barrier function of the epoxy coating efficiently through filling its porosities and defects [25,26]. Moreover, many oxygen functional groups present on the GO surface help adsorption of various active materials. In other words, GO serves as a nano container for active protection in the epoxy matrix [27–29]. On the other side, the outstanding properties of CNTs as one-dimensional nanomaterials with hollow tube structure such as large specific area, high aspect ratio, excellent chemical and thermal stability make them a good candidate for various characteristics to the polymeric coating [30–32]. Also, it has been reported in the literature that most of the papers published on the CNTs were related to the thermal, mechanical, and electrical properties [33–41]. Shon et al. scrutinized the influence of MWCNTs on the hydrophobic nature and water diffusion of the used epoxy matrix. They showed that the incorporation of MWCNT caused an increase in the hydrophobicity and water permeability of the epoxy coating [42]. Asmatulu et al. [43] reduced the UV degradation of the surface and augmented the polymeric coating lifespan by using MWCNT. Frankel [44] and Jeon [45] investigated the positive impacts of CNT utilization on various parameters such as corrosion control, wear resistance, and adhesion of the epoxy-based coatings on the carbon steel and aluminum alloy, respectively. The carbon nanotubes are expected to play a significant role in designing and manufacturing many nanomaterial devices in the future. Recently, they have been used in the electrochemical biosensors and sensors [33–37]. However, the limited compatibility and dispersion of CNT in most solvents hinder the easy usage of CNTs in many applications. There are some practical approaches to tackle this problem with CNTs, counting functionalization of the surface through intense oxidation [46], covalent bonding [47,48], and interaction with polymers [49–51].

Modification of CNTs with polymers to boost their dispersion stability, corrosion protection potency, and mechanical properties has recently received many researchers' attention. Among the polymers, the conductive ones, i.e., polyaniline, polypyrrole, and polydopamine, due to their excellent properties, are good candidates for acting as organic corrosion inhibitors to interact with the carbon nanotubes network for increased corrosion protection, electrical and mechanical properties [20,52–65]. The application of PANI has been extended due to its specific characteristics, such as environmental stability, low price, and corrosion protection properties [66–70]. Researches have shown that PANI plays a significant role in the anodic inhibition of corrosion with passivation layer formation [41–45]. Furthermore, the PANI's adsorption on the oxidized CNTs occurs by both covalently and electrostatic interactions because the PANI includes a positive charge, and oxidized CNT has a negative charge [65]. Akbarzadeh et al. [65] investigated the PANI's inhibition role on the CNT in the silane films on the mild steel surface. MWCNT solely can improve the waterborne acrylic films' adhesion to the steel substrate. Besides, it can reduce the matrix's porosity, which results in the anti-corrosion behavior of the acrylic coating. MWCNT could limit the water diffusibility and adsorption in the MWCNT/acrylic nanocomposite [71]. In similar research, 0.5% of CNT in the alkyd resin has shown good anti-corrosion properties and improved the carbon steel adhesion strength. High surface area and small size effect of CNT resulted in the barrier effect of the alkyd resin matrix [72]. Single wall CNT doped by polydopamine demonstrated high corrosion resistance by creating and manufacturing the thin and dense polydopamine layer. The layer hindered the cathodic reaction by adsorption of O_2 to the defect sites of CNT. Notably, the CNT edges have enough energy for being oxidized, making the penetration of the oxygen into the steel surface difficult. Therefore, it proves the CNT's excellent anti-corrosion potency due to its unique chemical structure [56]. Besides the good corrosion protection ability of the CNT-PANI nanocomposites in recent research, their active protection weakness has limited their pervasive application.

To the best of our knowledge, the influence of the usage of the modified multi-walled carbon nanotubes on the active corrosion protection has not been studied yet. Hence, in this study, we have aimed to evaluate the potency of the passive barrier and active self-healing roles of the zinc doped O-MWCNT-PANI nanoparticles in the EP coating for the first time. In this regard, first, the oxidized MWCNT was synthesized, and then the polyaniline was grafted on the O-MWCNT successfully. Afterward, the O-MWCNT-PANI was doped with zinc (Zn) ions in the optimum condition. The synthesized O-MWCNT-PANI-Zn was characterized by diverse characterization methods, including FT-IR, Raman spectroscopy, XRD, UV–vis spectrometer, FE-SEM-EDS, and TGA examinations. Furthermore, the active corrosion mitigation function of the synthesized nano-pigments in the solution phase was examined by EIS and polarization. The epoxy coating was formulated with 0.15 wt% nano-particles, and the coating corrosion resistance evaluation was done by EIS both on the intact and scratched films. The salt spray tests and cathodic delamination method were used to determine the corrosion control capability and adhesion properties, respectively.

2. Experimental

2.1. Raw materials

The MWCNTs, with a length of 1–10 μm and walls number of 3–15, were purchased from Nanostartech (Iran). Furthermore, the chemicals used for the oxidation of MWCNT, such as H_2SO_4 (98 wt%), and HNO_3, were procured from the Sigma-Aldrich Co. Ammonium peroxide sulfate $(NH_4)_2S_2O_8$, HCl (98 wt%), aniline, and zinc nitrate tetrahydrate were provided from Merck Co. The binder (i.e., epoxy) and hardener (polyamide) were purchased from Saba Co (IRAN). The mild steel (St-12) samples with the elemental composition of P = 1.2%, Mn = 1.1%, Si = 1.0%, Mo = 1.0%, Ni = 1.7%, Cr = 0.7% and Fe = 93.3% (wt.%) were obtained from MOBARAKEH ISFAHAN. The metal panels were mechanically abraded and ground with different sandpapers sizes, including 400 to 1200, and degreased by acetone, which was prepared from Mojallali Co. (Iran).

2.2. Synthesis of oxidized CNT (O-MWCNT)

The oxidizing process of MWCNTs was done with a 3:1 ratio of the combination of 100 ml of H_2SO_4 75% and HNO_3 65%, respectively. Then, 500 ppm MWCNT was put into the mentioned mixture and stirred at 100 °C for 12 h. The solution of acids and MWCNT was poured into 500 ml deionized water and mixed for 30 min in an ice bath. After that, a centrifuge (speed of 4000 rpm for 10 min) has been used to discrete the O-MWCNTs. Finally, the O-MWCNTs were washed and centrifuged several times by deionized water to bring pH to 6.

2.3. Fabrication and grafting polyaniline on the O-MWCNT

A 450 mg of O-MWCNTs was blended with 20 ml of 1 M hydrochloric acid, and then the prepared mixture was sonicated at 150 kW for 1 min. Concurrently, the mixture of 1.6 mM ammonium peroxide sulfate and 6.4 mM aniline in 30 ml of 1 M HCl was prepared. Afterward, the earlier prepared solution of O-MWCNT was put into the former solution gradually. The obtained mixture was agitated at room temperature for 24 h. Ultimately, the O-MWCNT-PANI was washed and centrifuged many times with distilled water to set the pH at 6.

2.4. Absorption of Zn ions on the O-MWCNT-PANI

500 ppm of OMWCNT-PANI was mixed with 50 ml DI water, while in the other beaker, 1000 ppm of zinc nitrate tetrahydrate was mixed with 50 ml purified H_2O simultaneously. Then, the two prepared mixtures were blended, and the pH was tuned to the range of 7–8, and mixing was continued for 30 min. Thereupon, the suspension was centrifuged and washed two times to get rid of the unreacted and un-adsorbed Zn ions. The syllogistic scheme of the synthesis procedure of nano-pigments is illustrated in Fig. 1.

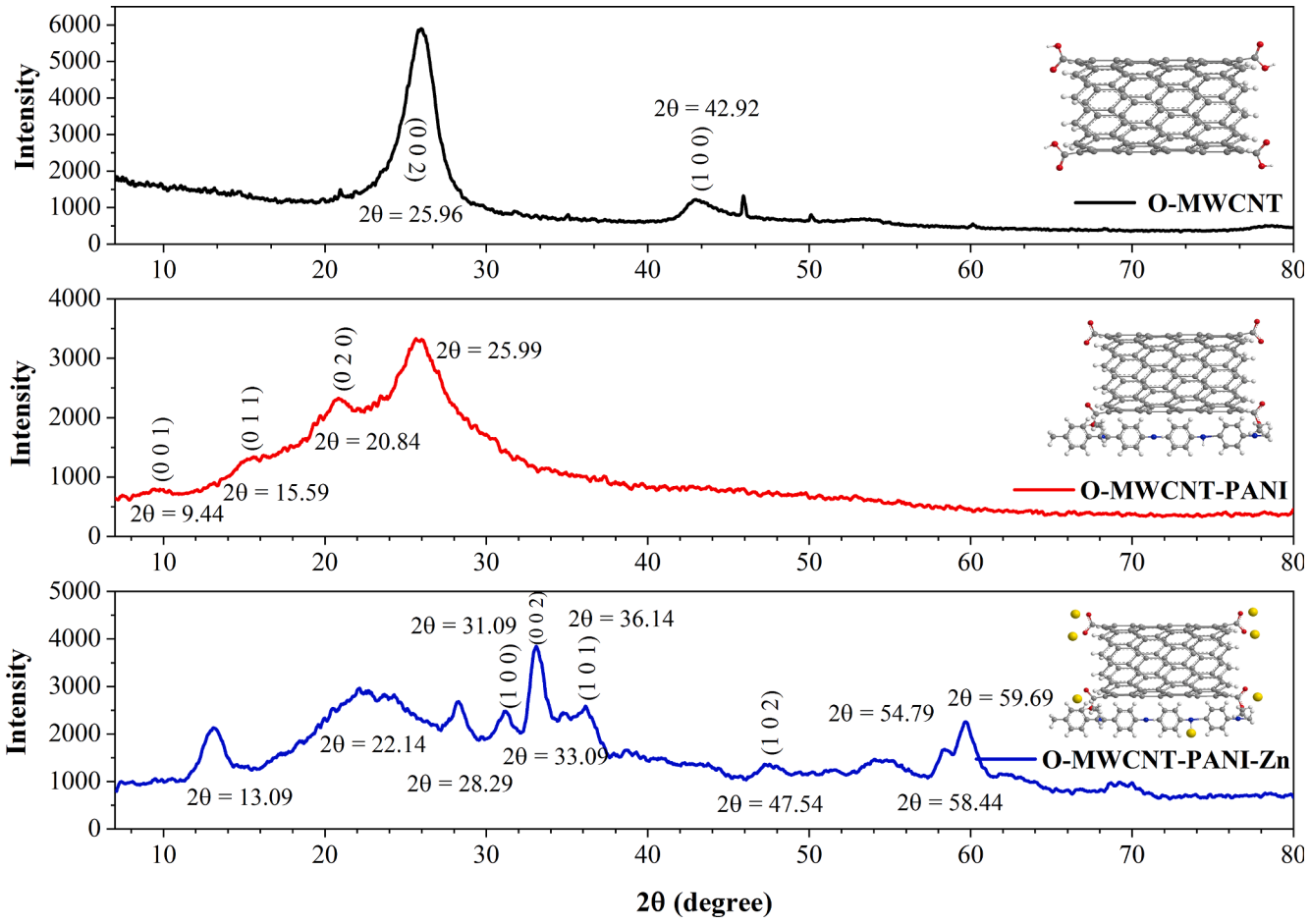

Fig. 2. X-ray diffraction of synthesized O-MWCNT, O-MWCNT-PANI, and O-MWCNT-PANI-Zn.

2.5. Preparation of the epoxy nanocomposite coating

0.15 wt% of each synthesized nanomaterial was first dispersed in 30 g epoxy resin in the presence of 5 ml toluene. The mixture was sonicated for 5-min to obtain a homogeneous particle dispersion in the epoxy resin and avoid aggregation. Successively, the obtained epoxy resin mixture was blended with a 23 g hardener under mechanical stirring. The provided nanocomposites were applied on the clean steel plates with a thickness of 70 μm. Primarily the coated plates were impounded at 25 °C for 72 h to obtain the skin-deep dry. After that, the plates were retained in the oven, adjusted at 80 °C for 1 h to acquire perfect curing. The neat epoxy coatings (without any nanomaterials) were prepared like the mentioned approach. They named the Blank sample in the next sections to better understand the influence of the synthesized nanoparticles.

2.6. Characterization

Determination of the chemical structure of the synthesized nanoparticles, which were carried out by the FTIR (Perkin Elmer model) technique, in the scope of 4000–400 cm^{-1} wavenumber. Defects and other information about the constructed nano-pigments were recognized by Raman spectroscopy, Xplora Plus model (excitation 532 nm) from Horiba scientific. The UV–vis spectrophotometer (CE9200) was utilized to determine the absorption properties and the interfacial interactions between O-MWCNT, PANI, and Zn cations. In order to analyze the phase amalgamation and d-spacing of the modified nanotubes, XRD was carried out by Philips device in the limited area of 7–80° (2θ) (made in the Netherlands). For estimating the morphology of the dried powders of the nano-pigments, and scanning the formed film on the metal panels immersed in the extracts, FE-SEM, which is equipped with EDS, was done with the help of MIRA3 TESCAN microscope. The TGA test was utilized to analyze the thermal stability and thermal decomposition of the specimens by the METTLER TOLEDO device, which worked in the range of 25 °C to 600 °C with a 10 °C/min heating rate in N_2 gas. The contact angle test was done via the homemade device to investigate the water propensity of the synthesized carbon-based nanotubes with scrutiny.

2.7. Electrochemical analyses

The extract of each synthesized nanomaterials (O-MWCNT-PANI and O-MWCNT-PANI-Zn) was prepared with 0.1 g mixing of each via 100 ml (3.5 wt%) saline media and mixed with a magnetic stirrer for 24 h continuously. After that, the admixtures were centrifuged, and the remaining topside solution was used as the extract. After the achievement of extracts, the steel panels covered by the beeswax-colophony blend with a subjected area of 1 × 1 cm were soaked in the acquired extracts to determine the anti-corrosion proficiency at specified immersion times. The measurements have been done with three electrodes, including SCE as a reference, graphite as auxiliary, and paradigms as working electrodes. Furthermore, the electrochemical properties of the epoxy-based coatings with and without artificial scratch were scrutinized by EIS.

Moreover, the polarization investigations were done (potential of ±200 mV and one $mV.s^{-1}$ rate of scanning). All the experiments were done with three repetitions to check the trustiness of the results. Regarding the electrochemical parameters, the acquired EIS plots were fitted by ZView 3.1 software. Besides, to reveal the coated samples' anti-

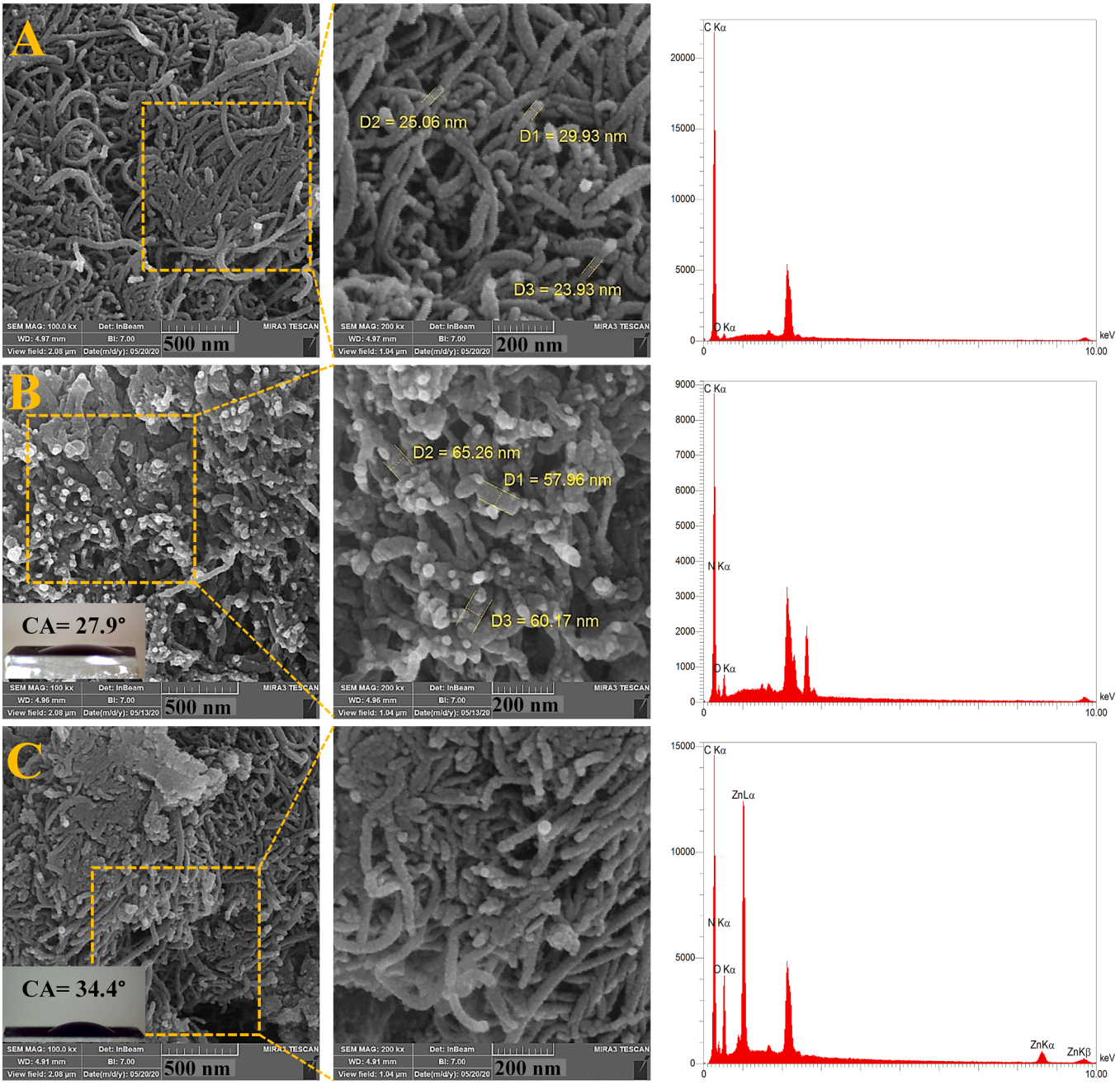

Fig. 3. FE-SEM images, contact angle and EDS of synthetized pigments: (A) O-MWCNT, (B) O-MWCNT-PANI (C) O-MWCNT-PANI-Zn.

Table 1
Atomic percentage of existing elements on the surface of O-MWCNT, O-MWCNT-PANI and O-MWCNT-PANI-Zn nano-pigments assessed by EDS Atomic percentage (%).

Elements	*O-MWCNT*	*O-MWCNT-PANI*	*O-MWCNT-PANI-Zn*
C	87.40	60.13	60.56
N	–	17.69	10.02
O	12.60	22.18	22.32
Zn	–	–	7.11

corrosion property with 0.15 wt% of nano-pigments, the salt spray test was done in 4 weeks. Besides, the cathodic delamination test was done to distinguish the adhesion trait of the coated samples, which is related to the corrosion resistance potency of the samples.

3. Results and discussion

3.1. Characterization techniques of synthesized carbon nano-pigments

Various characterization methods were used to analyze the synthesized nanoparticles which are explained in the supplementary information file. FTIR was done to study the PANI and zinc bonding to the O-MWCNT network. Fig. S1 illustrates the FTIR spectrum of the synthesized nanoparticles. UV–Visible spectroscopy was employed to vindicate the interfacial interactions among PANI molecules, O-MWCNT, and the zinc species adsorbed on O-MWCNT in an aqueous solution, which is illustrated in Fig. S2(a). The TGA was conducted to study the thermal resistivity of the synthesized nano-pigments. Fig. S2(b) and Table S1 display the remaining weight percent and DTG graphs of three nano-pigments versus temperature. The Raman plots of the nano-pigments are represented in Fig. S3. The ratios of the intensity of two prominent peaks in the first region (I_D/I_G) have been calculated and are given in Table S2 to have a better insight into the systemic modifications of different carbon nanotubes.

3.1.1. XRD spectroscopy

Delineation of polyaniline and zinc cations interactions with O-MWCNT and diffraction patterns of the synthesized nano-pigments are studied by XRD analysis (Fig. 2). There are two prominent peaks at $2\Theta = 25.96^\circ$ and $2\Theta = 42.92^\circ$ in O-MWCNT, corresponding to (002) and (100), which are imputed to the reflections of the in-plane regularity and interlayer spacing, respectively. In O-MWCNT-PANI, the peak corresponding to (002) became broader, and the intensity stepped down significantly. Furthermore, the distinct peaks of PANI at $2\Theta = 9.44^\circ$, 15.59°, and 20.84°, elucidating the prosperous grafting of PANI on the O-MWCNT, which are corresponded to the (001), (011), and (020), respectively. Unlike the XRD plots of O-MWCNT and O-MWCNT-PANI, the XRD diagram of O-MWCNT-PANI-Zn has many peaks in the range of $2\Theta = 30\text{-}50^\circ$. The peaks at $2\Theta = 31.09^\circ$, 33.09°, 36.14°, and 47.54° are consistent with (100), (002), (101), and (102), individually, are ascribed to the ZnO compound [61]. The outcomes of XRD are in good accordance with the Raman spectroscopy, showing the successful attachment of PANI and Zn ions on the O-MWCNT framework.

3.1.2. FE-SEM/EDS morphology observation and contact angle sizing

The morphological change and element composition in the synthesized nano-pigments were observed via the FE-SEM/EDS. The appearance and images of FE-SEM/EDS and contact angle of the synthesized powders are shown in Fig. 3. It is shown that the O-MWCNT (Fig. 3A) has endless and intertwined cord-like with smooth surface morphology, and the average diameter is approximately 20–30 nm. In contrast with the smooth surface of O-MWCNT, the grafting of PANI on the O-MWCNT surface led to the nanotubes with rough and uneven surfaces (Fig. 3B). The increase in the size of nanotubes to almost 60 nm is another reason that vouched for the successful growth of PANI on the plane of O-MWCNT. Furthermore, the O-MWCNT-PANI-Zn illustrated the resembling morphology to O-MWCNT-PANI with finer and less accumulated particles, which may be the influence of the electrostatic sorption of the zinc cations on the network of O-MWCNT-PANI. The EDS analysis affirmed the entity of Zn, N, O, and C elements, unfolding the favored deposition of PANI and Zn on the surface of O-MWCNT (Table 1). To evaluate the inherent hydrophilicity characteristic of the synthesized carbon-based nanotubes, the contact angle measurement was done. It can be seen that there was a little change in the contact angle of O-CNT-PANI and O-MWCNT-PANI-Zn samples. The contact angle of the O-MWCNT-PANI powder is about 27.9°, which can be ascribed to the polar nature of PANI on the network of O-MWCNT, which itself is embedded in several hydrophilic carboxylic groups. There was a meager increment in the contact angle of O-MWCNT-PANI-Zn nano-particles, which was about 34.4°. This might be credited to the adsorption of Zn cations on the polar groups of PANI and O-MWCNT.

3.2. Characterization of solution-phase and anti-corrosive characteristics of the synthesized pigments in extracts

In this section, the FTIR test was done to qualify the chemical structure of the layer of materials formed on the exposed area of the bare steel panel immersed in the extracts. Furthermore, the characterization of the phase composition of films formed on the steel panel immersed in the extracts was done via GIXRD analysis. FE-SEM/EDS illustrated the morphology and constituent atoms of the exposed metal surface to the extracts and saline solution. The contact angle test was applied to analyze the hydrophilicity degree of the immersed samples. The initial electrochemical characterization and corrosion protection potency of the carbon-based nano-pigments were measured using EIS and polarization analyses. All the analyses were done, as mentioned in the earlier sections.

3.2.1. EIS and polarization examinations

The deposition of the PANI-Zn or zinc cations on the modified O-MWCNT and the active inhibition capability of the synthesized nano-pigments was studied via the EIS method. EIS was employed in the solutions with and without O-MWCNT-PANI, O-MWCNT-PANI-Zn extracts with the uncovered area of 1 cm^2 of the steel panel in differing immersion times and intervals. The Nyquist and Bode graphic forms of EIS data are displayed in Fig. 4. The proper circuits were picked out for the specimens, and the obtained data from EIS were fitted with Zview software. The quantity of all acquired data is presented in Table 2. The one-time constant model was selected for the immersed steel panel in the blank saline solution, imputed to the charge transfer control of electrochemical reactions. There was a negligible increase of $\log |Z|_{10\ mHz}$ in O-MWCNT-PANI extract containing solution compared to the neat saline solution at all the immersion times apart from 1 h of immersion. This result could be ascribed to the fact that with PANI's attendance, an inhibitive layer that consists of metal oxide could be formed; however, the formed film was not sufficiently dense to protect the steel surface. Due to the structure of O-MWCNT and its limited active sites, a finite number of PANI molecules can be attached to the O-MWCNT network. Thus, the extract has a low amount of effective material consisting of O-MWCNT-PANI. However, PANI can affect the anodic reaction and mitigate the anodic sites. The oxidation process of the Emeraldine base structure of PANI to its Emeraldine salt form in the saline solution on the bare steel exposed area is probable. The Bode diagram corresponded to the solution with O-MWCNT-PANI-Zn extract illustrated two-time constant layout in which the first time constant, which is shown on higher frequencies, is related to the barrier function of the deposited film, while the other time constant observed at low frequencies is connected to the electrical double layer that took place at the junction of metal and electrolyte. The increase of R_T and $log|Z|_{10\ mHz}$ demonstrated the possible corrosion protection of the O-MWCNT-PANI-Zn. There can be two complementary mechanisms, including the passive

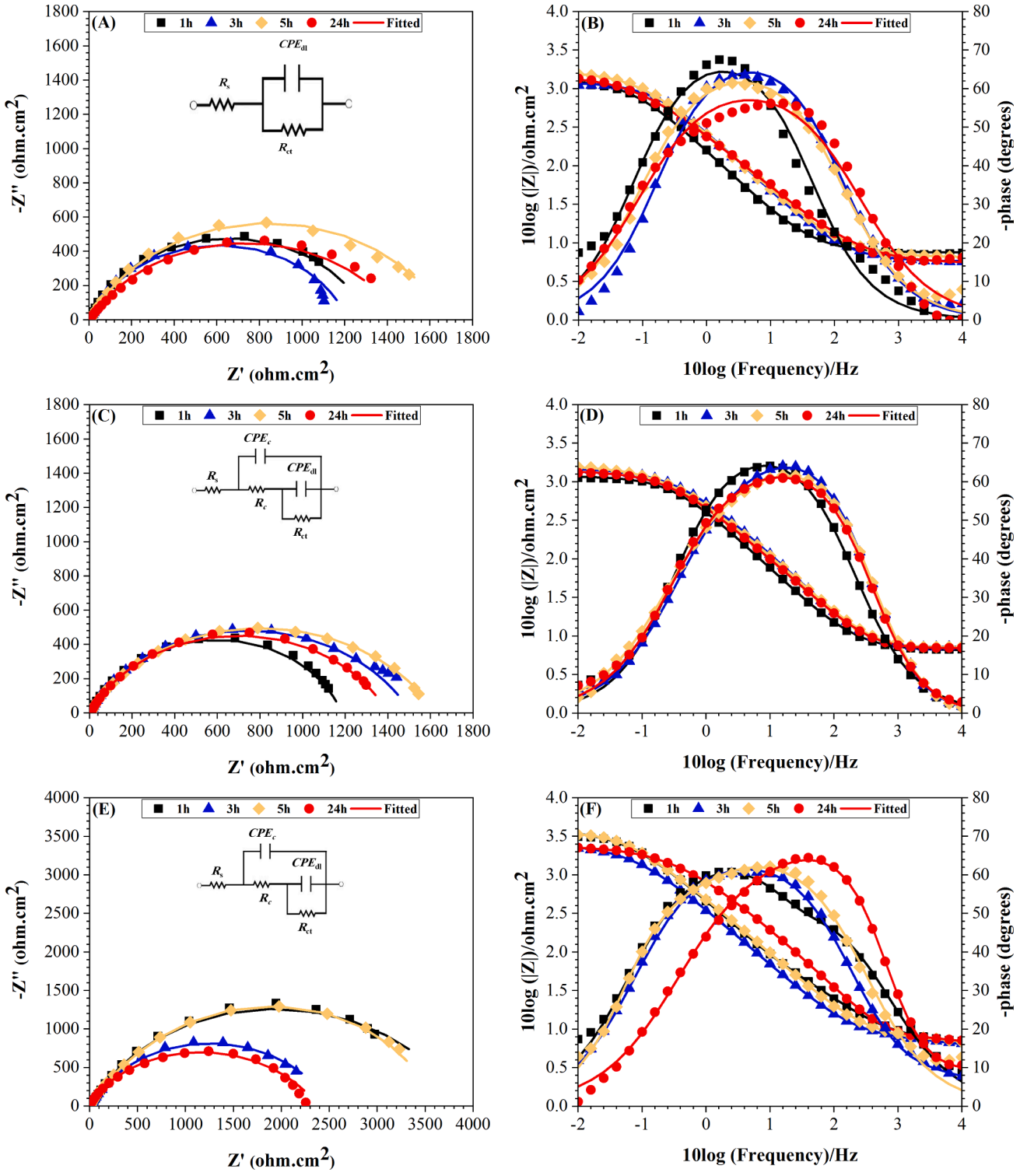

Fig. 4. Nyquist and Bode/Phase plots for steel panels exposed to extracts during immersion in saline solution: Blank (A, B), O-MWCNT-PANI (C, D), and O-MWCNT-PANI-Zn (E, F).

Table 2
Electrochemical impedance spectroscopy data of Blank, O-MWCNT-PANI, O-MWCNT-PANI-Zn extracts in 3.5% NaCl solution.

sample	*Time* (h)	R_s (ohm. cm^2)	CPE_c Q ($\times 10^{-4}$) ($ohm^{-1}.cm^{-2}.s^n$)	*n*	R_c (ohm. cm^2)	CPE_{dl} Q ($\times 10^{-4}$) ($ohm^{-1}.cm^{-2}.s^n$)	*n*	R_{ct} (ohm. cm^2)	R_T (ohm. cm^2)	$Log\|Z\|_{10mHz}$ ($ohm.cm^2$)
Blank	1	7.4	–	–	–	14.4	0.8	1302	1302	3.08
	3	5.7	–	–	–	8	0.79	1208	1208	3.06
	5	6.4	–	–	–	9.1	0.75	1670	1670	3.18
	24	5.4	–	–	–	10.5	0.7	1460	1460	3.11
O-MWCNT-PANI	1	6.4	–	–	–	4.85	0.8	1177	1177	3.06
	3	7.2	0.23	1	5.3	3.87	0.7	1497	1502.3	3.16
	5	7.2	0.18	1	4.1	4.65	0.68	1616	1620.1	3.19
	24	7	0.04	1	0.2	4.74	0.72	1392	1392.2	3.13
O-MWCNT-PANI-Zn	1	6.6	4.38	0.71	149	1.03	0.85	3725	3874	3.53
	3	5.4	3.07	0.68	3.06	3.93	0.77	2507	2510.06	3.53
	5	4	2.05	0.60	4.5	3.12	0.79	3990	3994.5	3.52
	24	5.2	2.6	0.63	4.1	0.29	0.97	2379	2383.1	3.35

Abbreviation 1. R_s: solution resistance, *n*: exponentioal constant, R_c: film resistance, R_{ct}: charge transfer resistance, R_T: total resistance, $|Z|_{10\ mHz}$: impedance at the lowest frequency

layer formation at the anodic sites of the bare steel panel in the presence of PANI [73] and the release of zinc cations at the cathodic areas and formation of zinc hydroxides and oxides. Thus, the anodic and cathodic reactions can be mitigated and controlled simultaneously. This means that the PANI grafted on the O-MWCNT framework is in its Emeraldine salt form. This Emeraldine salt form of PANI can be simply turned into its Emeraldine base form by grabbing the electrons generated via Fe's conversion to Fe^{2+}/Fe^{3+}. The bare steel immersion in the saline media of O-MWCT-PANI extract and Cl^- ions make the change in the PANI (Emeraldine base to Emeraldine salt and vice versa). The autocatalytic cycle can be completed, resulting in the stabilization of Fe in its passive form [52]. As shown in the previous sections, the zinc cations could bond with the O-MWCNT-PANI with either π-cation interactions or electrostatic adsorption. In both of these interactions, zinc cations can be released in the saline solution through the cation exchange with Na^+. It can be noted that by adsorption of PANI onto the O-MWCNT, a lot of negative sites of O-MWCNT would be occupied with PANI, and there would be a few accessible active sites for the attachment of zinc ions. Therefore, the complex and chelation amongst zinc cations and PANI molecules can be formed. However, the electrochemistry outcomes showed that the resulting nano-particles of PANI interactions and zinc cations with the O-MWCNT had the potency of active corrosion protection properties.

The corrosion protection mechanism was investigated via the potentiodynamic polarization method for different specimens after 48 h immersion in the saline solutions with and without extracts. The polarization plot is displayed in Fig. 5, and the extracted data from Tafel extrapolation are represented in Table 3. It is evident from the provided data that in the presence of nano-pigments extracts, not only the i_{corr} and corrosion rate decreased, but also E_{corr} shifted to more positive values. The results revealed that the synthesized nano-pigments had an active corrosion inhibition effect. There are three different corrosion protection mechanisms, including anodic, cathodic, and mixed, as dedicated to literature. If the value of E_{corr} is higher than 85 mV, then the mechanism of inhibition and protection would be either under anodic or cathodic control. However, when the amount of E_{corr} is lower than this value, then the corrosion inhibition mechanism is mixed with anodic and cathodic protection [74]. The remarkably reduction in the anodic and cathodic branches' slope of the extract of O-MWCNT-PANI, which are 0.060 V/dec and 0.096, respectively, indicated that the corrosion prevention is highly under mixed anodic and cathodic reactions control compared with the blank sample [75,76]. It means that the O-MWCNT and PANI's presence instantaneously affect the reactions that took place at cathodic and anodic spots likewise. In other words, the O-MWCNT can adsorb the oxygen molecules, which act as cathodic reaction control, and PANI can affix to the surface of the metal, reacting with metal oxides to stabilize the metal surface in its passive form [56]. Furthermore, in the solution with O-MWCNT-PANI-Zn extract, the E_{corr} reached the lowest value, describing the use of zinc hydroxide/oxide formation on the cathodic reaction mitigation. As considered, the cathodic spots can be protected by zinc hydroxide/oxide, and active anodic regions can be deterrent by the film formed with PANI, indicating the low corrosion rate of the sample exposed to the O-MWCNT-PANI-Zn extracts.

3.2.2. FTIR

The FTIR analysis revealed the major peaks of the formed chelate of the Zn cations and PANI on the steel panel surfaces. As shown in Fig. 6, exposure to the O-MWCNT-PANI and O-MWCNT-PANI-Zn extracts elucidated several peaks at 3430, 2920, 2850, 1630, 1387, 1033, and 576 cm^{-1}, ascribing to the OH, CH_2 stretching vibration, CH_3 stretching, C═C (aromatic), or C═N, COOH, C—N, and Fe—O or Zn—O, respectively [77,78]. The 1387 cm^{-1} peak, which had a weak vibration, was imputed to the COOH stretching vibration, indicating the successful grafting of PANI and Zn on the O-MWCNT. The vibrancy emerged between 2300 and 2400 cm^{-1} illustrated the formation of PANI-Fe^{2+}/Fe^{3+} and PANI-Zn^{2+} complexes on the steel plates [79]. Furthermore, the C—N vibration at 1033 cm^{-1} shifted to the lower wavenumbers in the O-MWCNT-PANI-Zn sample, which might be another evidence of complexes' formation among PANI and Fe^{2+}/Zn^{2+} ions [79]. Moreover, the peak located in the vicinity of 805 cm^{-1} is allocated to the Zn—O amalgam [74], elucidating PANI and Zn cations' constitution.

3.2.3. GIXRD test achievements

The grazing X-ray diffraction pattern of the immersed steels in the extracts in the presence of the mentioned saline solution has shown in Fig. 7. As shown, several compounds are illustrated in the patterns, including Fe, α-Fe_2O_3 [80,81], α-FeOOH [82], and β-FeOOH [83]. The O-MWCNT-PANI-Zn extract indicated other peaks such as Zn $(OH)_2$, $ZnFe_2O_4$, FeOCl, $Fe_6Cl_{2-x}(OH)_{12+x}$, and $Zn_5(OH)_8Cl_2H_2O$ (Simonkolleite). The 2Θ degree and various reference peaks are provided in Table 4. Simonkolleite has an appropriate anti-corrosive characteristic, resulting from the dispersal of zinc in the NaCl solution. Furthermore, by introducing nano-pigments, the intensity of the Fe^{2+} peak has increased dramatically. It might be the medium for interactions amongst the pigments and metal panel surface, bringing prospering adsorption of nano-pigments on the metal via the interaction of PANI molecules' nitrogen heteroatoms with vacant orbital of Fe and zinc cations. Moreover, the π-cation interchange took place between the zinc cations and PANI, thus some peaks' intensity and 2Θ degree shifted. All in all, the consequences of the grazing XRD were in common with the FTIR achievements.

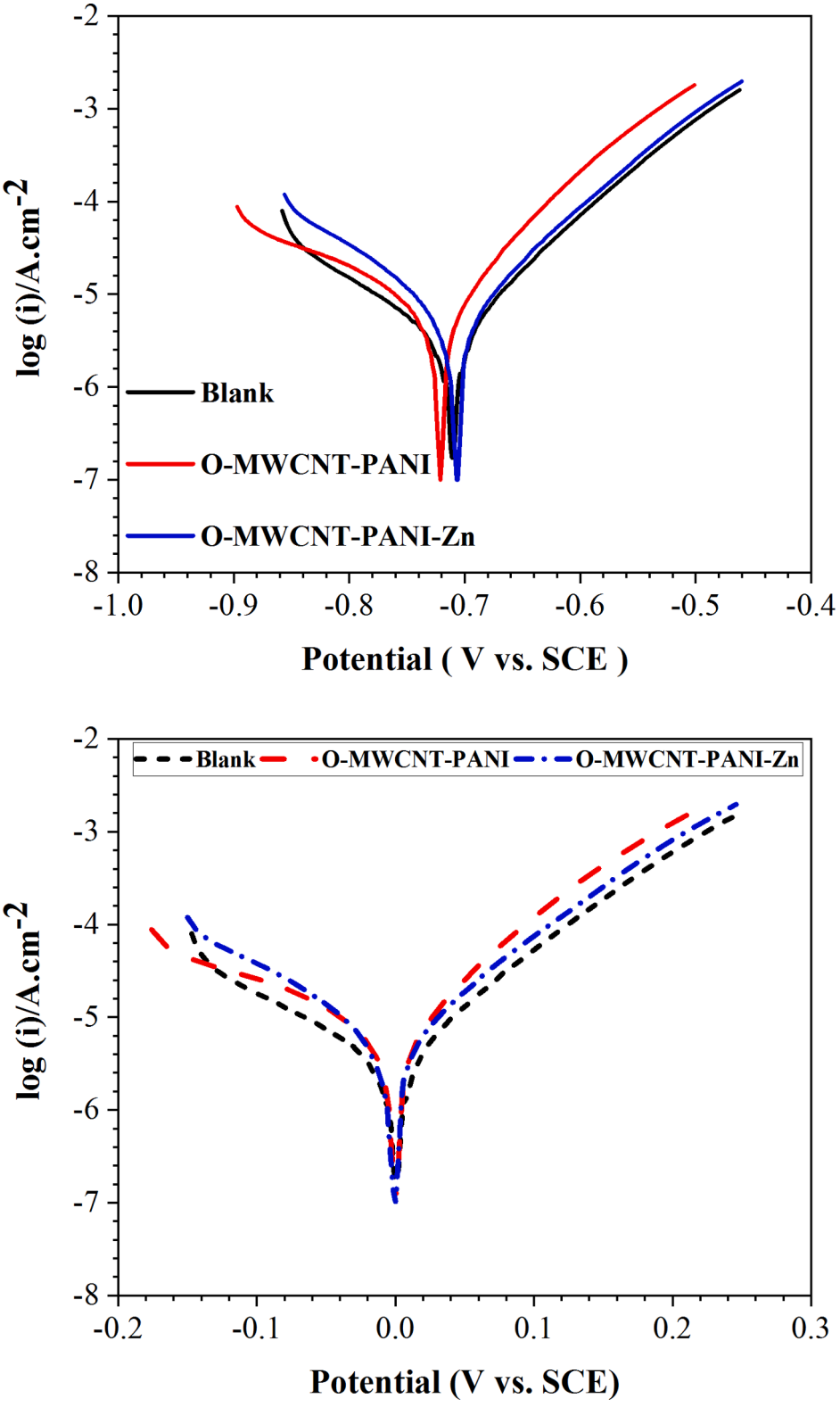

Fig. 5. Potentiodynamic plot of O-MWCNT-PANI, O-MWCNT-PANI-Zn extrats in 3.5% NaCl solution.

Table 3
Tafel extrapolalted data of Blank, O-MWCNT-PANI, O-MWCNT-PANI-Zn extracts in 3.5% NaCl solution.

sample	E^1_{corr} vs SCE (V)	i^2_{corr} (μA/cm^2)	β^3_a (V/dec)	β^4_c (V/dec)	*Corrosion* Rate (mm/year)
Blank (NaCl)	−0.73	8.13	0.088	0.199	0.026
O-MWCNT-PANI	−0.7212	3.75	0.060	0.096	0.012
O-MWCNT-PANI-Zn	−0.7079	2.39	0.054	0.060	0.007

E_{corr}: corrosion potential
i_{corr}: corrosion current density
β_a: anodic Tafel slope
β_c: cathodic Tafel slope
[1] The standard deviation varied between 3% and 7%
[2] The standard deviation varied between 5% and 8%
[3] The standard deviation varied between 4% and 9%
[4] The standard deviation varied between 5% and 9%

3.2.4. *FE-SEM/EDS morphology analysis and contact angle sizing of immersed samples*

The FE-SEM-EDS images and contact angle data of the bare metal immersed in the mentioned saline solutions with and without nanoparticles extracts are shown in Fig. 8. The steel panels' morphological images showed that the rust formed on the surface, causing a planar structure related to the disparate iron oxides or iron hydroxides. The morphology of the film formed on the metal surface after exposure to the extracts was distinct from the film formed in the neat saline solution. In O-MWCNT-PANI extract, the PANI molecules were observed. The O-MWCNT-PANI FE-SEM image indicated the release of PANI from the O-MWCNT frame. Fig. 8(C) illustrated that the PANI molecules or Zn were randomly distributed on the metal's surface. Furthermore, the EDS mapping showed the atom percentage (Table 5) in different specimens and ascertained the previous results about the release of inhibitors from the O-MWCNT. In contrast with the neat saline solution exposed panel, the two other steel panels showed nitrogen atoms. Besides, the presence of zinc cations in the extract containing O-MWCNT-PANI-Zn confirmed the release of organic-inorganic compounds. The contact angle results of the immersed samples exhibited that the incorporation of the nanopigments had affected the water propensity. The bare steel panel, which was immersed in the neat saline solution, displayed the lowest contact angle. It is due to the hydrogen bonding between the metal oxides and the electrolyte, which caused surface heterogeneities, hence, a lower contact angle [84]. The O-MWCNT-PANI extract demonstrated a lower contact angle compared with the O-MWCNT-PANI-Zn, relating to the more polar groups of O-MWCNT or PANI, which was a reason for hydrogen bonding between the O-MWCNT-PANI and electrolyte. The O-MWCNT-PANI-Zn extract has increased the contact angle impressively from about 50° to a value around 80°. This alteration in contact angle value is imputed to the isolation of active spots of the metallic surface, which is occurred by the interaction of zinc cations with the metal surface. These outcomes were well aligned with the powders' GIXRD and contact angle results, as mentioned above.

3.3. *Anti-corrosion virtues and characteristics of the provided epoxy-based nanocomposites*

3.3.1. *EIS exploration*

The EIS exploitation was utilized to better understand the active/barrier corrosion inhibition performance of the prepared 2 × 2 cm area of the cured coatings with 1 cm artificial scratch and 1 × 1 cm area of the intact cured nanocomposite coatings. It should be noted that all coatings (Blank/EP, O-MWCNT/EP, O-MWCNT-PANI/EP, and O-MWCNT-PANI-Zn/EP) used for the electrochemical analysis had the same thickness of about 70 ± 5 μm. The artificial scratch is made by a sharp cutter to reach the surface of the steel sheet. The surface of the steel is visually seen in all scratched coatings. Therefore, the depth of the scratch is 70 ± 5 μm in all samples. The remaining part of the samples and steel plates were

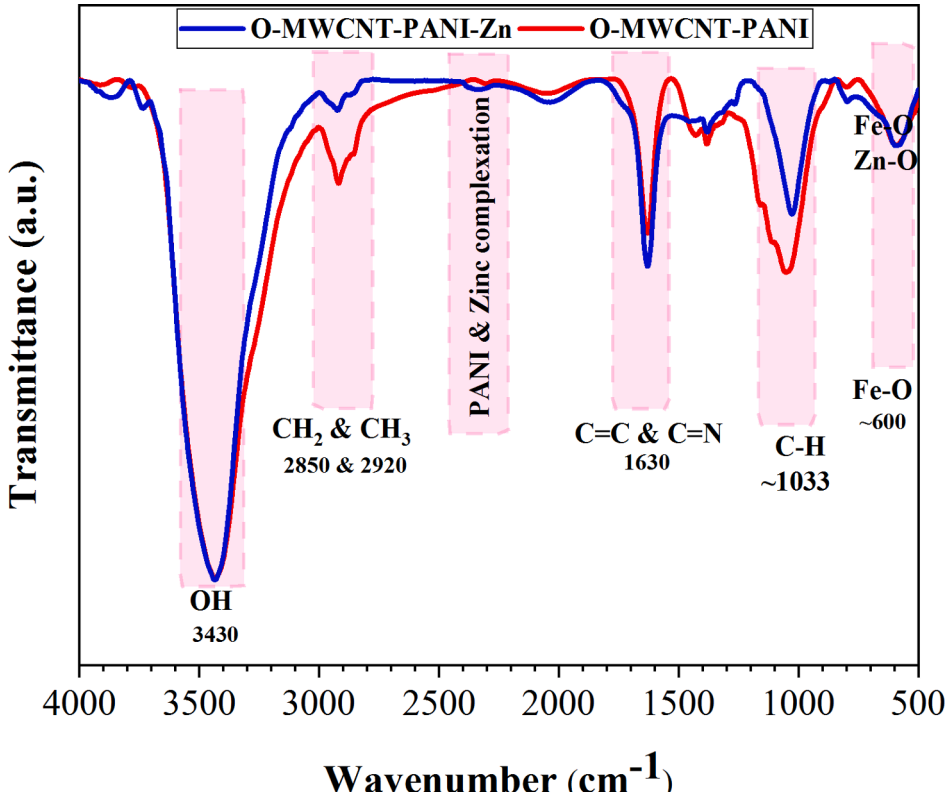

Fig. 6. FTIR spectroscopy of formed film on bare metals immersed 24 h in O-MWCNT-PANI, O-MWCNT-PANI-Zn extracts in 3.5% NaCl solution.

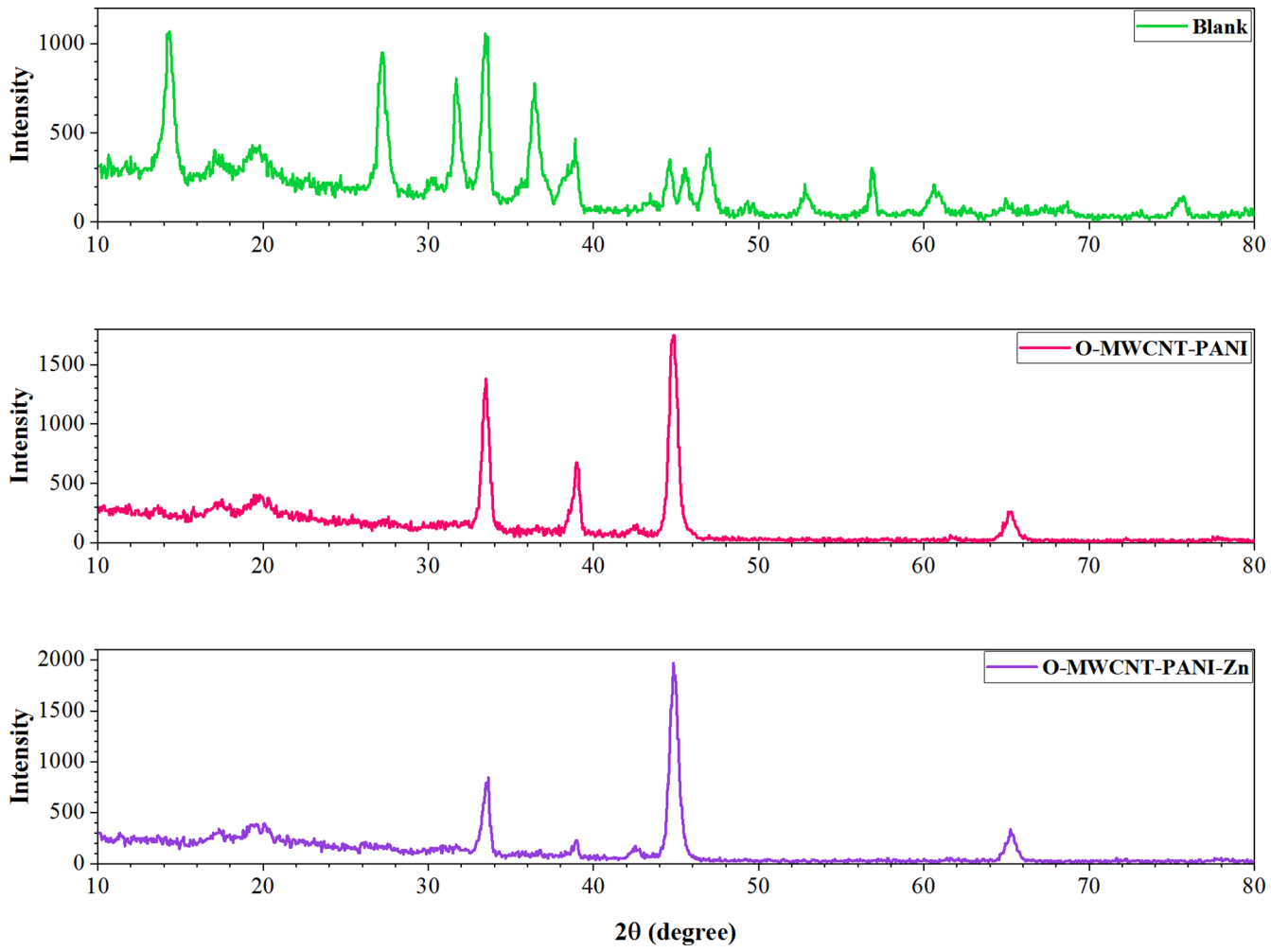

Fig. 7. GIXRD analysis of the steel panels immersed 24 h in saline solution with and without O-MWCNT-PANI and O-MWCNT-PANI-Zn extracts.

Table 4
Name and phase characteristic of various 2Θ values extracted from GIXRD plot.

Sample	Detected structure/ phase	Chemical Formula	JCPDS card no	2θ value
Blank	Hematite	Fe_2O_3	00–032-0469	33.15
	Magnetite	Fe_3O_4	96–900-2330	44.75, 64.85
	Iron	Fe	01–087-0722	44.75, 64.85
O-MWCNT-PANI	Hematite	Fe_2O_3	00–032-0469	33.49
	Iron	Fe	01–087-0722	44.84, 65.19
	Iron (III) Oxide chloride	FeOCl	96–101-0310	11.89, 20.34, 33.49, 38.94
	Iron chloride hydroxide	$Fe_6Cl_{2-x}(OH)_{12+x}$	00–049-0095	11.89, 20.34, 33.49, 38.94
O-MWCNT-PANI-Zn	Hematite	Fe_2O_3	00–032-0469	33.64
	Magnetite	Fe_3O_4	96–900-2330	44.84, 65.24
	Iron	Fe	01–087-0722	44.84, 65.24
	Iron chloride hydroxide	$Fe_6Cl_{2-x}(OH)_{12+x}$	00–049-0095	11.34, 20.04, 33.64, 38.89
	Zinc hydroxide chloride hydrate	$Zn_5(OH)_8Cl_2H_2O$	01–077-2311	11.34, 20.04, 33.64, 38.89
	Iron (III) Oxide Chloride	FeOCl	96–101-0310	11.34, 20.04, 33.64, 38.89
	Zinc hydroxide	$Zn(OH)_2$	12–0479	38.89
	Franklinite	$ZnFe_2O_4$	96–900-6904	31

covered to inhibit the diffusion of water and corrosive ions to other areas. The specified zone of the prepared samples was subjected to a corrosive saline solution, and the measurement was done at defined immersion times. The Nyquist and Bode diagrams of diverse coatings with artificial scratch were illustrated in Fig. 9. Meanwhile, the fitting data were presented in Tables 6 and 7. Fig. 9 shows that by increasing the immersion time, the diffusion of the corrosive ions, such as Cl^- and Fe^{2+} from the electrolyte into the scratch, may occur. The corrosion (electrochemical anodic and cathodic) reactions took place at the interface of the coatings and steel plate. It can be seen that loading the nanocontainers into the epoxy resin, have had a significant influence on the $log|Z|_{10\ mHz}$, which is the vital parameter, illustrating the corrosion protection property of various coatings. In this case, the O-MWCNT-PANI-Zn loaded epoxy coating showed the highest $log|Z|_{10\ mHz}$ around 5.06 ohm.cm^2, which is corresponded to the control of electrochemical reactions at the cathodic and anodic places. Moreover, the O-MWCNT-PANI/EP and O-MWCNT-PANI-Zn/EP samples had the highest charge transfer resistances of about 24,149 and 122,670 ohm.cm^2, respectively,

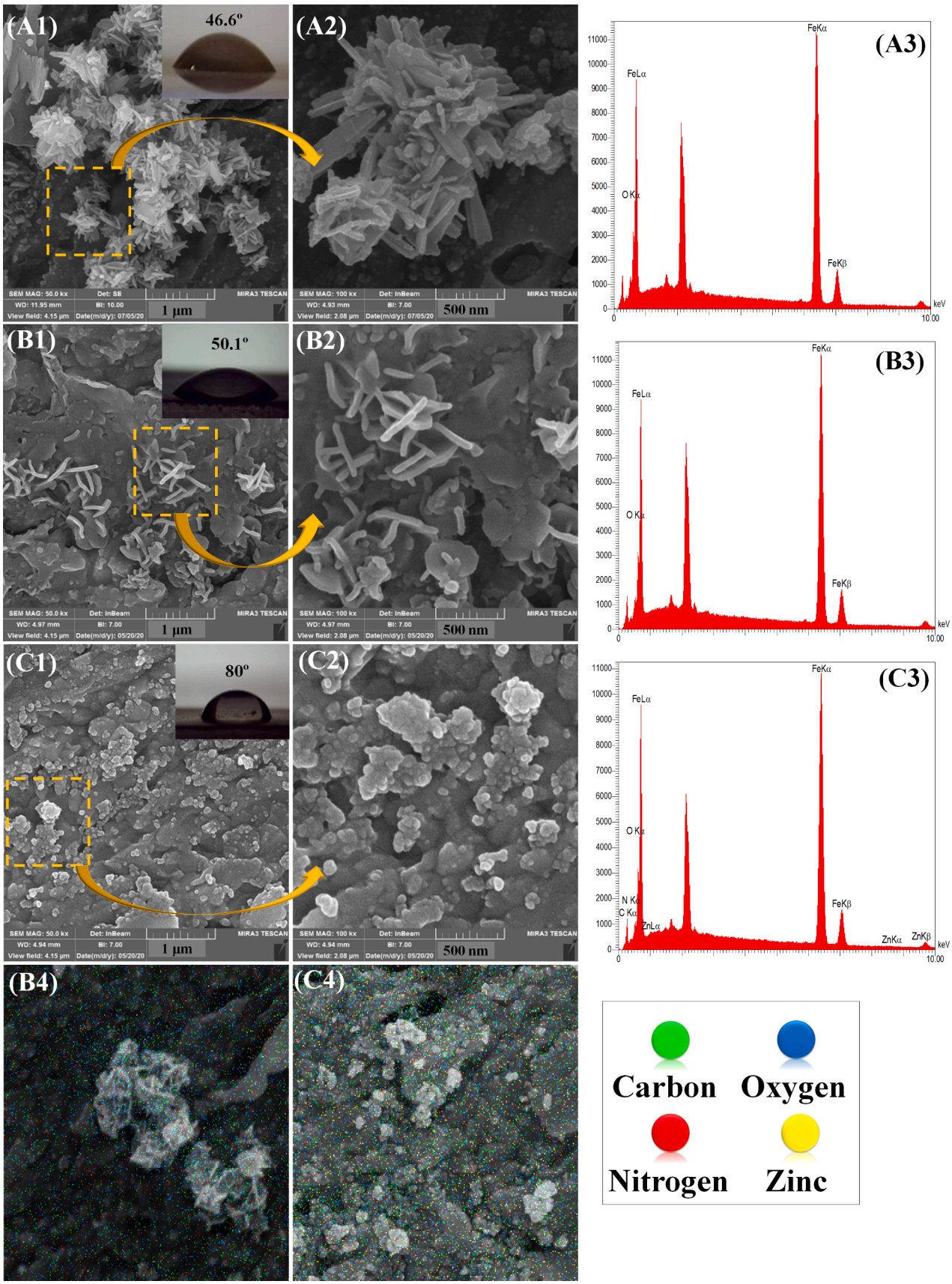

Fig. 8. FE-SEM images, EDS-mapping and contact angle of mild steel surface immersed in: (a1, a2, a3) saline solution, (b1, b2, b3, b4) O-MWCNT-PANI extract and (c1, c2, c3, c4) O-MWCNT-PANI-Zn extracts for 24 h: morphology and structures of film formation on the surface of mild steel.

Table 5
Atomic percentage of existing elements on the surface of mild steel immersed in saline solution and O-MWCNT-PANI and O-MWCNT-PANI-Zn extracts assessed by EDS Atomic percentage (%).

Elements	*Blank*	*O-MWCNT-PANI*	*O-MWCNT-PANI-Zn*
C	–	21.14	28.17
N	–	7.31	6.67
O	17.97	12.78	11.5
Fe	82.03	58.76	49.72
Zn	–	–	3.94

at the optimized time. It describes the relation of charge transfer control to the electrical double layer formation at the metallic surface. The high value of charge transfer resistance confirms the adsorption of inhibitors at the scratch and cathodic/anodic points. At the same time, the heterogeneity index is a symptom of the inhibitive layer appearance. The more the heterogeneity index, the more the homogenous inhibitive film. It is evident from the data provided in Table 6 that the heterogeneity index of O-MWCNT-PANI-Zn/EP was in the vicinity of 1, which confirmed the uniform and dense film formation composed of zinc hydroxide and PANI-Fe complexes. The corrosion control and self-healing capability of the O-MWCNT-PANI/EP and O-MWCNT-PANI-Zn/EP nanocomposite coatings can be discussed as the suppression of the reactions at cathodic and anodic zones likewise in the presence of PANI and zinc cations. PANI is a conductive polymer in its Emeraldine salt form, and it can attach to the surface of the metal. It would play a catalyzer role in the oxidation reaction on the metal surface [85]. Thus, as mentioned previously, it can form a dense passive layer composed of Fe_2O_3 and Fe_3O_4 species, protecting the metal and limiting further corrosion [85]. Moreover, the PANI's autocatalytic performance makes the metal surface stabilized in its passive region [52]. Also, zinc cations and hydroxyl groups' reactions may occur in the cathodic region, creating a zinc hydroxide compound [73]. In this manner, both anodic and cathodic reactions could be mitigated by loading nano-pigments that form the organic-inorganic complexes.

The barrier function and the smart corrosion inhibition potency of the obtained nanocomposite coatings were assessed by EIS measurement of the intact coatings without any scratches, as illustrated in Fig. 10. The observation of Fig. 10 illustrated that with the increase in the immersion time, the frequency region, illustrating the capacitive function moved to the elevated frequencies for the pristine epoxy coatings. It shows the diffusion of the corrosive ions, including Cl^- and Fe^{2+} from the electrolyte, into coating through its porosities and pits, influencing its barrier performance. However, the coatings with nano-pigments showed better corrosion protection properties with higher capacitive characteristics. The summit of the phase angle did not vary remarkably within the period of the measurement. The impedance magnitudes at low frequencies after seven weeks of immersion in the harsh 3.5% NaCl solution for the blank/EP, O-MWCNT/EP, O-MWCNT-PANI/EP, and O-MWCNT-PANI-Zn/EP were 10^7, 10^{10}, $10^{10.3}$, and $10^{10.8}$ ohm.cm^2, respectively. Also, the maximum value of the phase angle at topmost frequencies is another symptom of the coatings' good barrier function [74]. After almost 10 weeks of immersion, the coatings with nano-pigments had a maximum phase angle around 90°; however, the blank/EP coating phase angle reached 74° in 7 weeks of immersion, illustrating the low barrier proficiency of the pristine epoxy coating. The nano-pigments filled coating with O-MWCNT showed better active/barrier corrosion protection properties than the neat epoxy coatings. It is because of the mitigation of the cathodic reaction in the presence of O-MWCNT. The O-MWCNT could adsorb oxygen in the electrolyte, and the concentration of O_2 would be declined in the electrolyte, which results in the cathodic reaction suppression [56]. The lowest resistive region is ascribed to the coatings with O-MWCNT-PANI and O-MWCNT-PANI-Zn nano-pigments.

Furthermore, the breakpoint frequency, which is connected to the tiny exfoliated area at the coating/metal interface [99], took place at 45° and moved to the higher frequencies in the blank/EP than the coatings with nano-pigments. The higher $log|Z|_{10\ mHz}$ and lower breakpoint frequency in the coatings with nano-pigments illustrate the active and barrier corrosion inhibition characteristics. Although the epoxy coatings have been used widely due to their excellent characteristics in this experiment, the neat epoxy showed the lowest corrosion protection ability. This circumstance might be attributed to the entrance of ions to the coating/metal interface and permeability characteristics, resulting in the cathodic and anodic reactions. In other explanations, the generated Fe^{2+} and Fe^{3+} ions can react with Cl^- ions of saline solution to set the anodic spots' pH to an acidic level [74]. Also, the hydroxyl ions at the cathodic area may interact with Na^+ ions to create Na(OH), causing the basic nature creation at cathodic sites. Thus, the saponification of the coatings can be resulted from the pH increment at cathodic points and decrement at anodic points, breaking the hydrogen bonds (which may be occurred by the diffusion of water to the boundary) across the coating and metallic surface. However, it is known that the higher the nano-pigments interfacial area and aspect ratio, the path of the diffusion of corrosive ions may become more zigzagging and tortuous so that the permeability will become reduced [86], and the release of inhibitors can also happen.

3.3.2. *Anti-corrosion mechanism*

3.3.2.1. The inhibition mechanism of solution phase. The effect of zinc cations and PANI molecules is displayed in Fig. 14. Due to the presence of dissociable protons of PANI molecules (N–H^+), i.e., Emeraldine salt structure, the protonated amine is dominant in the neutral pHs. That is to say; the anodic spots possess negative charges because of the production of electrons through the anodic reactions. Thus, the electrostatic adsorption between the negatively charged steel surface in the anodic points and the positively charged amino groups of the PANI (Emeraldine salt) resulted in the formation of Leuco-Emeraldine form compounds. Regarding the production of Fe^{2+} at the anodic surface, the iron cations and the zinc cations present in the electrolyte led to a complex production with the organic inhibitor (PANI) via the electron sharing process, resulting in an insoluble product. The product can precipitate on the anodic surface and mitigate the anodic reactions. Besides, the zinc hydroxide/oxide precipitation on the cathodic zones completed the steel surface coverage and avoided the direct contact between the corrosive electrolyte and the electrode [87]. The polarization results also confirmed the effect of O-MWCNT-PANI and O-MWCT-PANI-Zn extracts on both anodic and cathodic slopes. Indeed, the decrement of the cathodic slope in O-MWCNT-PANI is related to the presence of O-MWCNT. The O-MWCNT can react with the O_2 molecules in the electrolyte and mitigate the cathodic reactions. The detailed description of the O-MWCNT function has been explained in the section describing the anti-corrosion properties of the scratched coatings.

3.3.2.2. The inhibition mechanism of coating phase. By comparing each of the fabricated nanocomposites (O-MWCNT/EP, O-MWCNT-PANI/EP, and O-MWCNT-PANI-Zn/EP) with the Blank/EP, the role of O-MWCNT, O-MWCNT-PANI, and O-MWCNT-PANI-Zn is described in both scratched and intact coatings in Fig. 11.

The scratched coatings and self-healing mechanism clearly showed that the incorporation of the O-MWCNT did not significantly affect the corrosion resistance based on the EIS results. The total resistance ($R_T = R_c + R_{ct}$) of the Blank/EP and O-MWCNT/EP did not change noticeably during the immersion time. However, the important issue is the considerable difference between the R_{ct}, which can be related to the suppression of the cathodic reaction by O-MWCNT due to its O_2 absorption capability. This capability lowers the O_2 concentration in the cathodic regions and subsequently increases the R_{ct} [56]. Grafting PANI on the O-MWCNT resulted in the enhancement of both R_c and R_{ct}. PANI

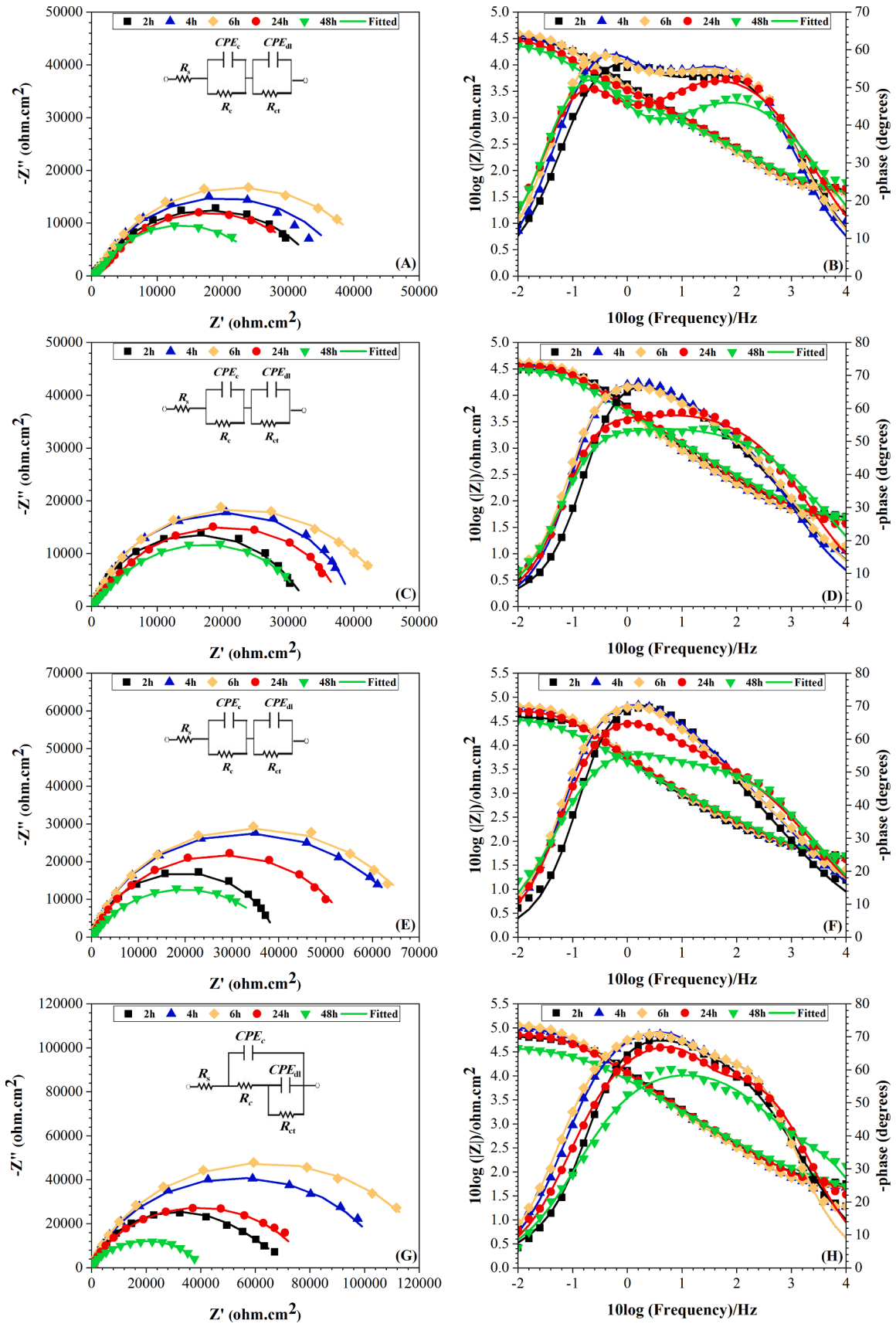

Fig. 9. Nyquist and Bode/Phase plots for coatings with artificial scratch during 48 h immersion in saline solution: Blank/EP (A, B), O-MWCNT/EP (C, D), O-MWCNT-PANI/EP (E, F), and O-MWCNT-PANI-Zn/EP (G, H).

Table 6
Electrochemical impedance spectroscopy data of Blank/EP, O-MWCNT/EP, O-MWCNT-PANI/EP, O-MWCNT-PANI-Zn/EP scratched coatings in 3.5% NaCl solution.

Sample	Time (h)	R_s (ohm.cm^2)	CPE_c Q ($\times10^{-4}$) (ohm^{-1}.cm^{-2}.s^n)	n	R_c (ohm.cm^2)	CPE_{dl} Q ($\times10^{-4}$) (ohm^{-1}.cm^{-2}.s^n)	n	R_{ct} (ohm.cm^2)	R_T (ohm.cm^2)
Blank/EP	2	36.9	0.60	0.80	33666	0.89	0.65	1077	34743
	4	33.9	0.69	0.84	37605	0.86	0.67	1270	38875
	6	31.2	0.74	0.86	41776	0.89	0.66	1643	43419
	24	31.3	1.22	0.84	30502	0.73	0.63	2741	33243
	48	28.1	1.51	0.84	24377	0.93	0.59	1657	26034
O-MWCNT/EP	2	37.5	0.37	0.96	25061	1.76	0.53	8613	33674
	4	35.9	0.49	0.99	32000	1.3	0.60	8000	40000
	6	31.6	0.52	0.95	32695	1.7	0.56	15998	48693
	24	33.4	0.56	0.91	32000	0.80	0.62	6000	38000
	48	27.5	0.74	0.86	26154	0.97	0.57	6225	32379
O-MWCNT-PANI/EP	2	34.7	0.35	0.94	35000	3.25	0.48	5000	40000
	4	28.6	0.36	0.91	57952	3.57	0.46	31558	89510
	6	28	0.37	0.91	60562	3.26	0.46	24149	84711
	24	29.8	0.39	0.86	54041	1.91	0.52	1210	55251
	48	30.2	0.61	0.74	37870	2.18	0.52	889.5	38759.5
O-MWCNT-PANI-Zn/EP	2	51.6	0.13	0.80	1299	0.031	0.92	66025	67324
	4	44.6	0.17	0.80	4100	0.016	1	104590	108690
	6	44.8	0.17	0.80	4287	0.018	1	122670	126957
	24	43	0.18	0.75	3363	0.016	0.99	75773	79136
	48	31.2	0.06	0.78	123.7	0.244	0.66	40500	40623.7

Table 7
Impedance at low frequency and phase angle at high frequency data of Blank/EP, O-MWCNT/EP, O-MWCNT-PANI/EP, O-MWCNT-PANI-Zn/EP scratched coatings in 3.5% NaCl solution.

Sample	Time (h)	$Log\|Z\|_{10mHz}$(ohm.cm^2)	-Phase angle at 10 kHz
Blank/EP	2	4.5	12.7
	4	4.55	10.6
	6	4.59	12.3
	24	4.46	15.9
	48	4.36	18.6
O-MWCNT/EP	2	4.5	14.1
	4	4.59	11
	6	4.63	13.8
	24	4.56	15.8
	48	4.48	21.2
O-MWCNT-PANI/EP	2	4.58	13.8
	4	4.8	16.7
	6	4.82	17.7
	24	4.72	18
	48	4.53	18.6
O-MWCNT-PANI-Zn/EP	2	4.81	14.6
	4	5	9.04
	6	5.06	9.07
	24	4.86	13.8
	48	4.56	27.2

could improve the compatibility of O-MWCNT-PANI with the epoxy matrix compared with the O-MWCNT since O-MWCNT contains many oxygen-containing functionalities in its structure. These functionalities negatively affected the particle dispersion in the polymeric matrix [49].

Moreover, the release of PANI in the anodic region (as discussed earlier in the Polarization results) could suppress the anodic reaction. PANI is a conductive polymer in its Emeraldine salt form, and it can attach to the surface of the metal. Therefore, it would play a catalyzer role in the oxidation reaction on the metal surface [85]. Thus, as mentioned previously, it can form a dense passivating layer composed of Fe_2O_3 and Fe_3O_4 species, protecting the metal and limiting further corrosion [85]. Moreover, the PANI's autocatalytic performance makes the metal surface stabilized in its passive region [52]. These happenings on the metal surface led to an increment of R_{ct} in O-MWCNT-PANI/EP compared to the O-MWCNT/EP. Finally, doping of zinc cations on the O-MWCT-PANI boosted the R_T dramatically in EIS results. The R_T reached the maximum (126957 ohm.cm^2) value in 6 h immersion time. The long-term release of zinc cations and their chelation with PANI were seen in 24 h and 48 h immersion times. Compared to O-MWCNT-PANI, the R_T parameter increased from 55,251 to 79,136 ohm.cm^2 in 24 h immersion in the presence of O-MWCNT-PANI-Zn, which showed moderate/controlled release of zinc/PANI species. This release was continued until 48 h for the O-MWCNT-PANI-Zn/EP since the R_T was higher than the O-MWCNT-PANI/EP in 48 h. This enhancement showed the zinc cations' active role in corrosion protection by forming stable zinc hydroxides and Zn/PANI complex compounds on the cathodic/anodic region of the metal surface [73]. The proof of the formed film's stability in the scratched zone is the heterogeneity index (n) derived from the EIS results, which was near 1 in O-MWCNT-PANI-Zn/EP. The total resistance comparison between the solution phase and scratched coatings versus different immersion times were depicted in Fig. S4. The figure illustrates the difference between solution and coating phases clearly.

Regarding the effect of O-MWCNT, PANI fibers, and Zn cations on the coatings' barrier properties, it should be noted that the incorporation of O-MWCNT into the epoxy matrix lengthened the pathway of electrolyte to reach the metal/coating interface. The PANI grafting improved the dispersion of O-MWCNT, which proved a higher impedance magnitude after 10 weeks of immersion. Finally, the modification of O-MWCNT-PANI with zinc cations led to a high modulus hybrid organic-inorganic structure making strong interfacial strength with the polymeric matrix. Moreover, the micro-voids and cracks in the coating (if present) are protected by zinc cations in the near vicinity.

In addition, the contact angle gauging of the prepared free films is illustrated in Fig. 12. It is apparent from the images that the inclusion of nano-pigments into the nanocomposite coatings had a significant influence on the water propensity of the specimens. That is to say, the contact angle of the Neat/EP coating, O-MWCNT/EP, O-MWCNT-PANI/EP, and O-MWCNT-PANI-Zn/EP were 63.3°, 76.1°, 79°, and 82.5°, respectively. The O-MWCNT nanoparticles have more polar and hydrophilic groups (i.e., COOH) than O-MWCNT-PANIs, which are responsible for the lower contact angle of O-MWCNT-PANI/EP in comparison with O-MWCNT/EP nanocomposite coatings. On the contrary, by doping Zn cations on the O-MWCNT-PANI framework, the N–H polar groups of PANI can be suppressed with zinc atoms, causing the less hydrophilic characteristic.

3.3.3. *FE-SEM/EDS mapping of an artificial scratch of epoxy nanocomposites*

The morphology and EDS mapping obtained from the artificial

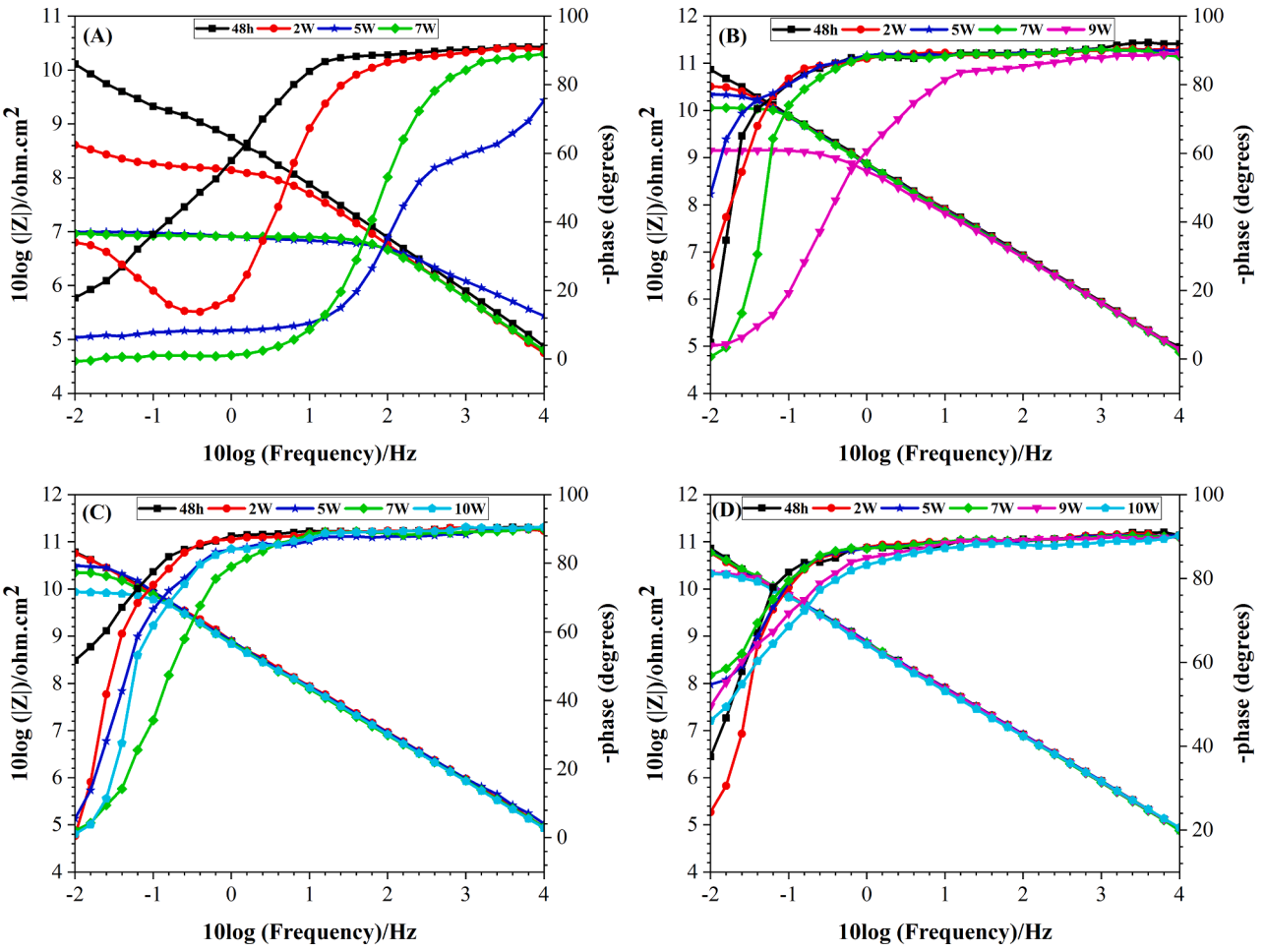

Fig. 10. Bode/Phase angle diagram of intact coatings in 3.5% wt NaCl solution for 10 weeks. (A) Blank/EP, (B) O-MWCNT/EP, (C) O-MWCNT-PANI/EP, (D) O-MWCNT-PANI-Zn/EP.

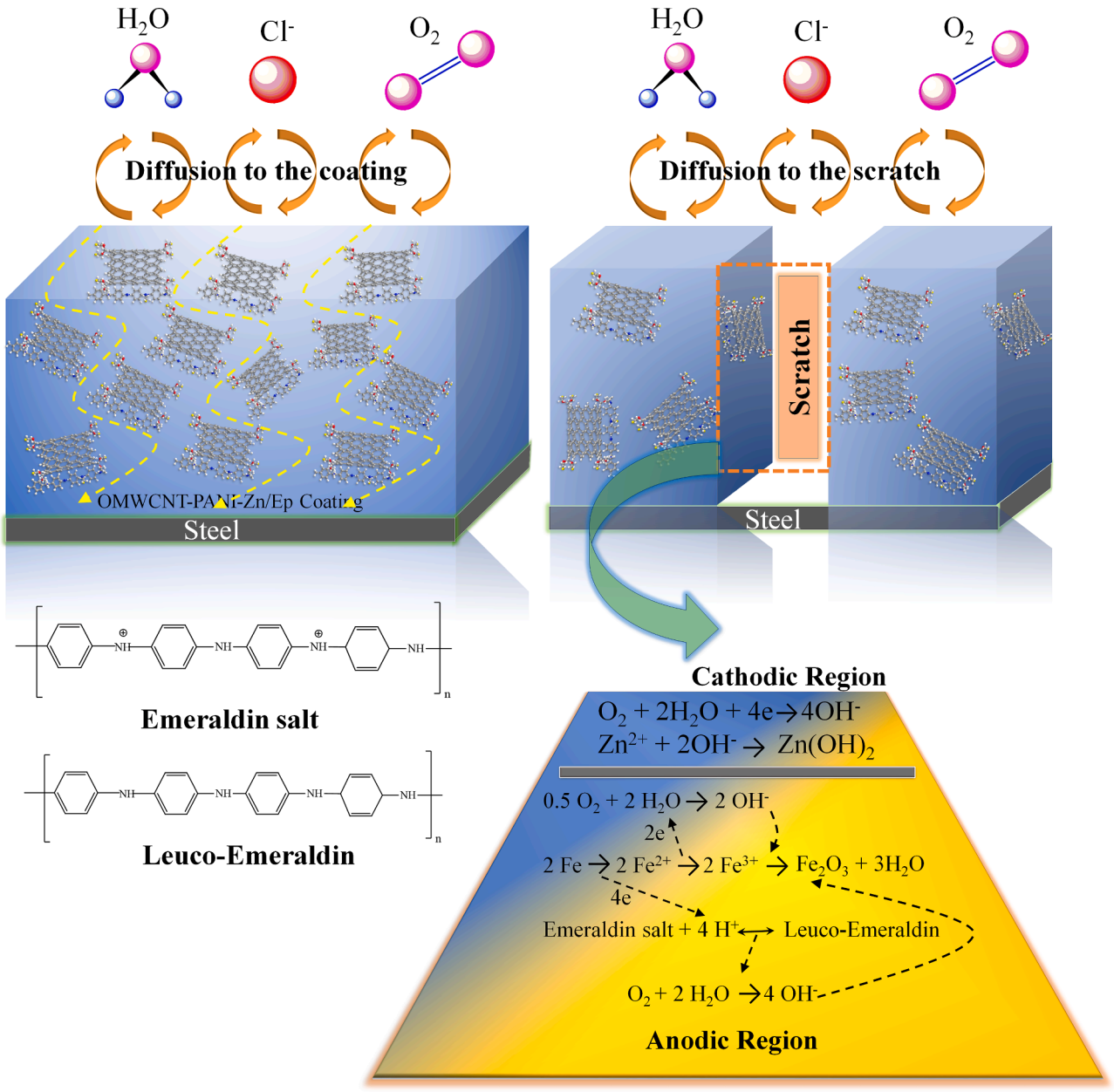

Fig. 11. Schematic illustration of active and barrier protection of O-MWCNT-PANI-Zn/EP nanocomposite.

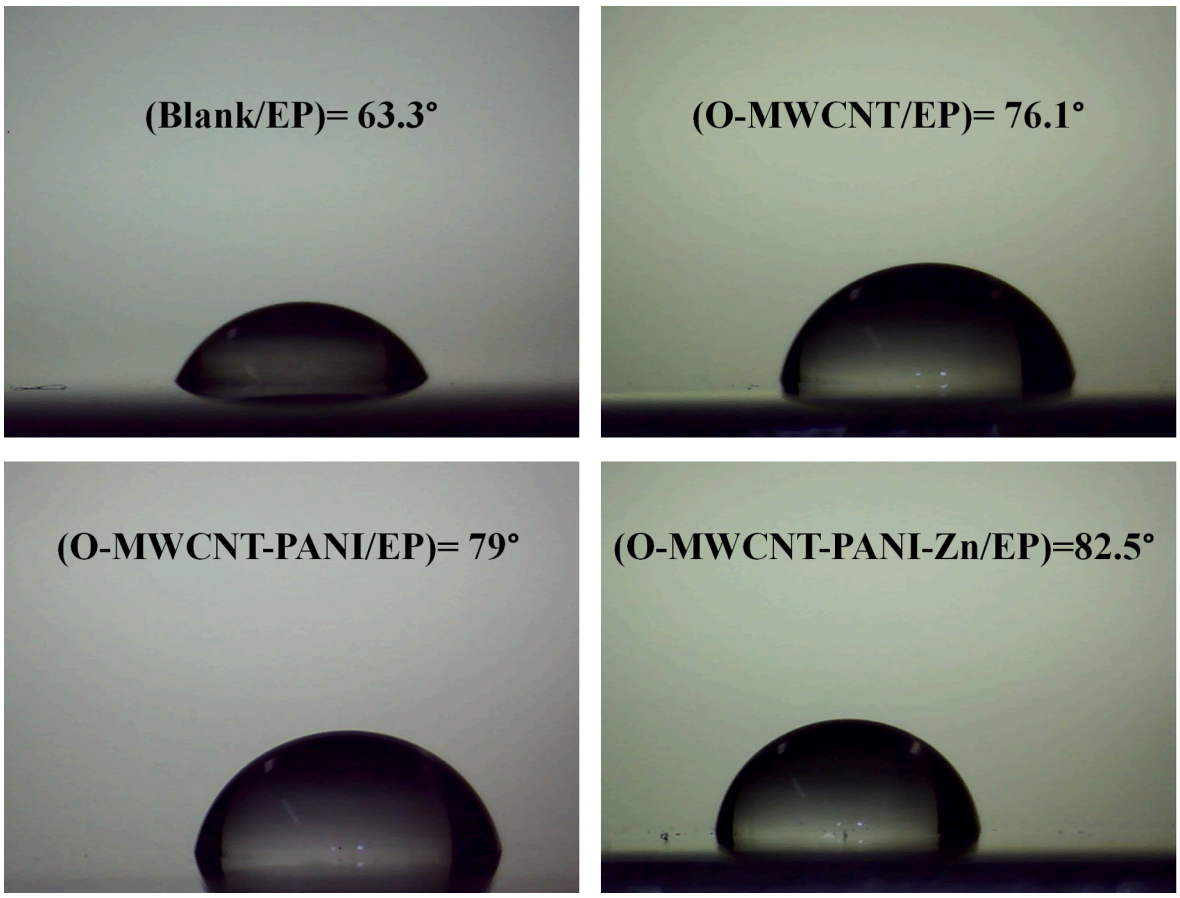

Fig. 12. The contact angle sizing of the prepared nanocomposites and the Neat/EP.

scratch settled on the prepared nanocomposite coatings after 48 h immersion in the mentioned saline solution is illustrated in Fig. 13. Visual observations of the immersed specimens demonstrated the foundation of corrosion products in and around the scratch zone in the pristine epoxy and O-MWCNT/EP coatings. The FE-SEM images showed the corrosion product generation in both blank/EP and O-MWCNT/EP coatings. However, the morphology of two other obtained nanocomposite coatings (O-MWCNT-PANI/EP and O-MWCNT-PANI-Zn/EP) was different. According to Fig. 8, the zinc cations and PANI fibers are demonstrated in the shape of compact balls and fibers, respectively. These kinds of morphologies are illustrated in Fig. 13 (c and d), which indicated the PANI and zinc cations presence at the scratch zone. The metal's corrosion in the presence of corrosive ions (Cl^-) was mitigated through applying the coatings with O-MWCNT-PANI and O-MWCNT-PANI-Zn nano-pigments, which might be owing to the formed passive layer with PANI and zinc hydroxide/oxide molecules on the metal surface and the scratch site, which mitigated the anodic and cathodic reactions. Therefore, the products in the scratch region of the defected O-MWCNT-PANI-Zn/EP coatings were in the form of zinc hydroxide/oxide, which resulted in the healing process of the scratch and improved the corrosion conservation capability more impressive than the O-MWCNT-PANI/EP sample. This occurrence might be due to the principle that organic corrosion inhibitors have less protection efficiency than the inorganic ones in neutral media [88]. The EDS mapping also approved the FE-SEM and electrochemical analysis results too. The Fe/O ratio was in the vicinity of 0.059 in the blank/EP coating, and increased to almost 0.28 in O-MWCNT-PANI-Zn/EP coating, which indicates the lower corrosion products formation [89]. Additionally, nitrogen and zinc atoms displayed in the specimens' EDS spectra are along with the successful release of PANI molecules and zinc cations, which are represented in Table 8.

3.3.4. Salt spray and cathodic delamination analyses

The salt spray test was also carried out to investigate the nanocomposite coatings' anti-corrosion performance in harsh conditions. Perceivable observations of different nanocomposite coatings have been done for 4 weeks (Fig. 14). A glance at the images provided by salt spray illustrated that the neat epoxy and O-MWCNT/EP coatings had lower corrosion protection performance and more corrosion products formed neighboring the artificial scratch. Furthermore, the corrosion products are observed out of scratch too. However, the O-MWCNT-PANI/EP and O-MWCNT-PANI-Zn/EP coatings revealed better protection and lower products. The corrosion spots and products' volume is remarkably less than the other two specimens in scratch and around it, illustrating the better corrosion inhibition property. As discussed, the results confirmed the obtained data from the electrochemical evaluations. The cathodic delamination was used to study the effect of nano-pigments in the nanocomposite coatings. The 9 cm^2 of each coating with a 4 mm diameter hole in the center was subjected to the saline solution for about 24 h. Then, the radius of the disjunct coating from the steel panel was determined. The more the radius, the less the adhesion property. The radius computation has been done with three repetitions to check the reliability of the results. Fig. 15 demonstrated the images of the coating disbonding, and the results of the computed radiuses are given in Table 9. By adding carbon-based nano-pigments to the coating, the radius decreased substantially. There can be various reasons for that happening. One might be the reasonable distribution of the nano-pigments in the epoxy resin. Another one can be due to the potent chemical bonding through the epoxy resin and the metal surface in the presence of the nano-pigments. Besides, in the coating without O-MWCNT-PANI-Zn particles, the electrolyte diffusion into the coating/metal interface resulted in the coating delamination resulting from the cathodic reaction, pH rise beneath the coating, and corrosion products

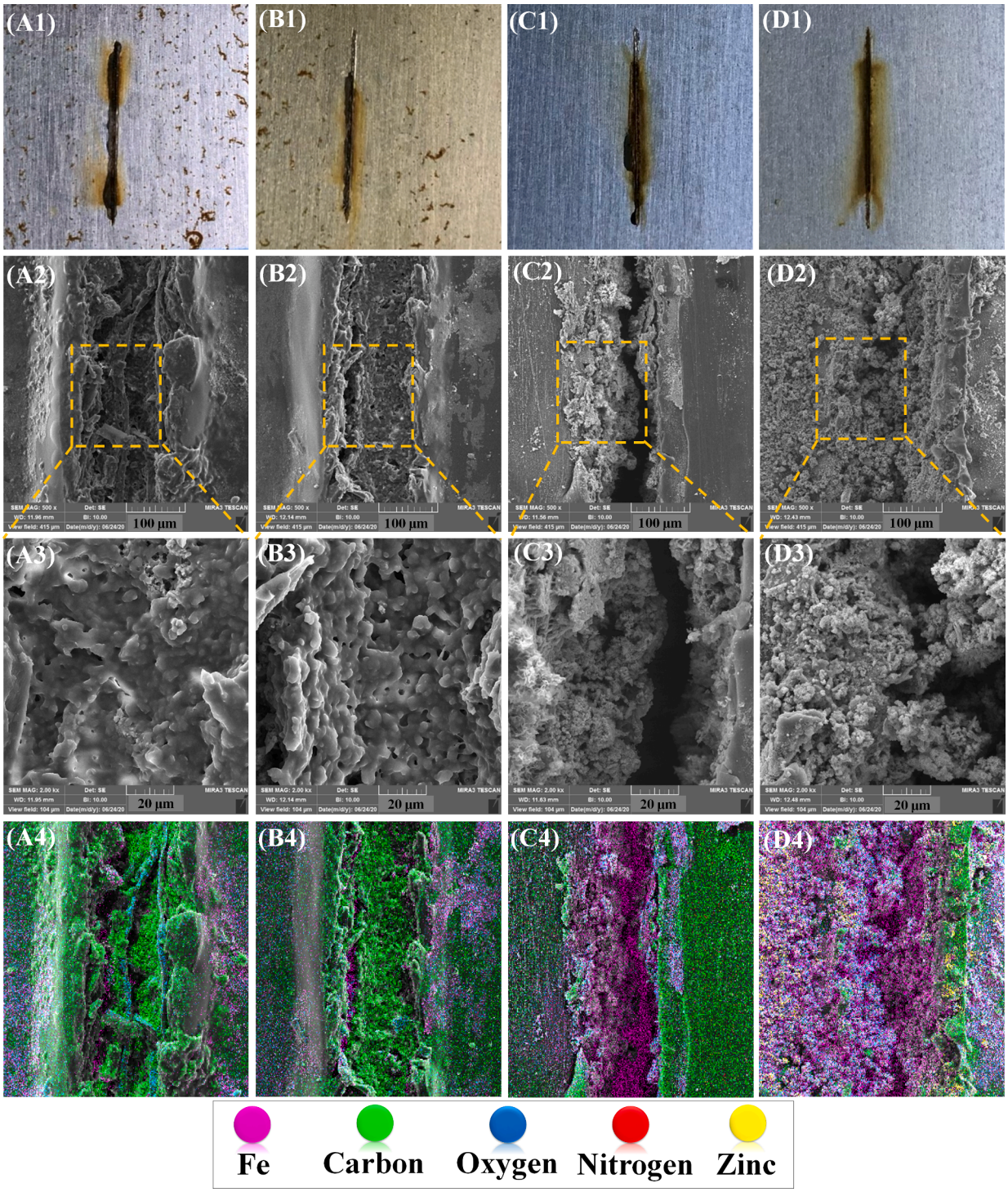

Fig. 13. FE-SEM images and EDS mapping of the scratch zone of coatings immersed in saline solution for 48 h: (a1-a4) Blank/EP, (b1-b4) O-MWCNT/EP, (c1-c4) O-MWCNT-PANI/EP, (d1-d4) O-MWCNT-PANI-Zn/EP.

Table 8
Atomic percentage (%) of existing elements in the scratched zone of coatings assessed by EDS.

Elements	*Blank/EP*	*O-MWCNT/EP*	*O-MWCNT-PANI/EP*	*O-MWCNT-PANI-Zn/EP*
C	74.16	73.09	61.17	36.89
N	–	–	5.32	3.68
O	24.40	25.22	26.96	44.22
Fe	1.44	1.69	6.56	12.46
Zn	–	–	–	2.76

creation. However, the O-MWCNT-PANI-Zn particles, due to PANI and Zn film's presence, could protect the defected site and prevent the coating delamination from the substrate. These observations depicted that in the presence of O-MWCNT-PANI-Zn particles, the barrier properties, and active inhibition performance could be enhanced.

According to Fig. 11, the PANI and Zn film could inhibit the anodic and cathodic reactions by forming a passive film with the mechanism given. In this way, the cathodic reaction rate, which is responsible for the increase of pH beneath the coating, and the anodic reaction rate responsible for the creation of corrosion products, can be significantly decreased. So, the coating delamination from the defected site could be reduced in this way. Also, in the presence of O-MWCNT-PANI-Zn particles, the coating barrier properties could be enhanced due to the particle's high specific surface area, providing a zigzagging diffusion pathway. The mentioned reasons could reduce corrosion product propagation in the nanocomposites, causing lower cathodic delamination. It means that the O-MWCNT-PANI-Zn could significantly affect the interfacial interactions between the coating and metal substrate.

4. Conclusion

A multi-walled carbon nanotube was oxidized and then modified with polyaniline and zinc nitrate tetrahydrate to obtain carbon-based nano-pigments. The synthesized nano-pigments were characterized by different methods, including FTIR, UV–Vis, Raman, TGA, XRD, and FE-SEM/EDS. Furthermore, the dual active/barrier anti-corrosion capability of the samples in the solution phase with extracts and in the prepared nanocomposite coatings with and without scratch was studied by EIS. The results obtained by characterizing the synthesized nano-pigments revealed that PANI has successfully grafted mostly via covalent bonding on the O-MWCNT framework and then the zinc cations with π-cation interactions or electrostatic adsorption victoriously stacked to O-MWCNT-PANI network. After that, the electrochemical and potentiodynamic polarization examination of the O-MWCNT-PANI and O-MWCNT-PANI-Zn extracts showed that both of them mitigated the corrosion rate compared with the blank saline solution. The results ascertained that the O-MWCNT-PANI-Zn/EP coating had the highest corrosion protection of about 10 weeks while the neat epoxy and O-MWCNT/EP's resistance decreased to almost 7 weeks and 9 weeks, respectively. The salt spray and FE-SEM/EDS results evidenced the fewest corrosion product formation in both O-MWCNT-PANI/EP and O-MWCNT-PANI-Zn/EP coatings. It was due to the release of PANI, zinc, and the formation of PANI-metal complexes (passivation of the metal surface) or zinc hydroxide/oxide impact layer on the metal surface. Moreover, the cathodic delamination showed the utmost coating disbondment in the neat epoxy and the highest coating adhesion in O-MWCNT-PANI-Zn/EP, which may be ascribed to the enhancement of the interfacial interactions amongst the epoxy binder and steel surface with the help of O-MWCNT-PANI-Zn nano-pigments.

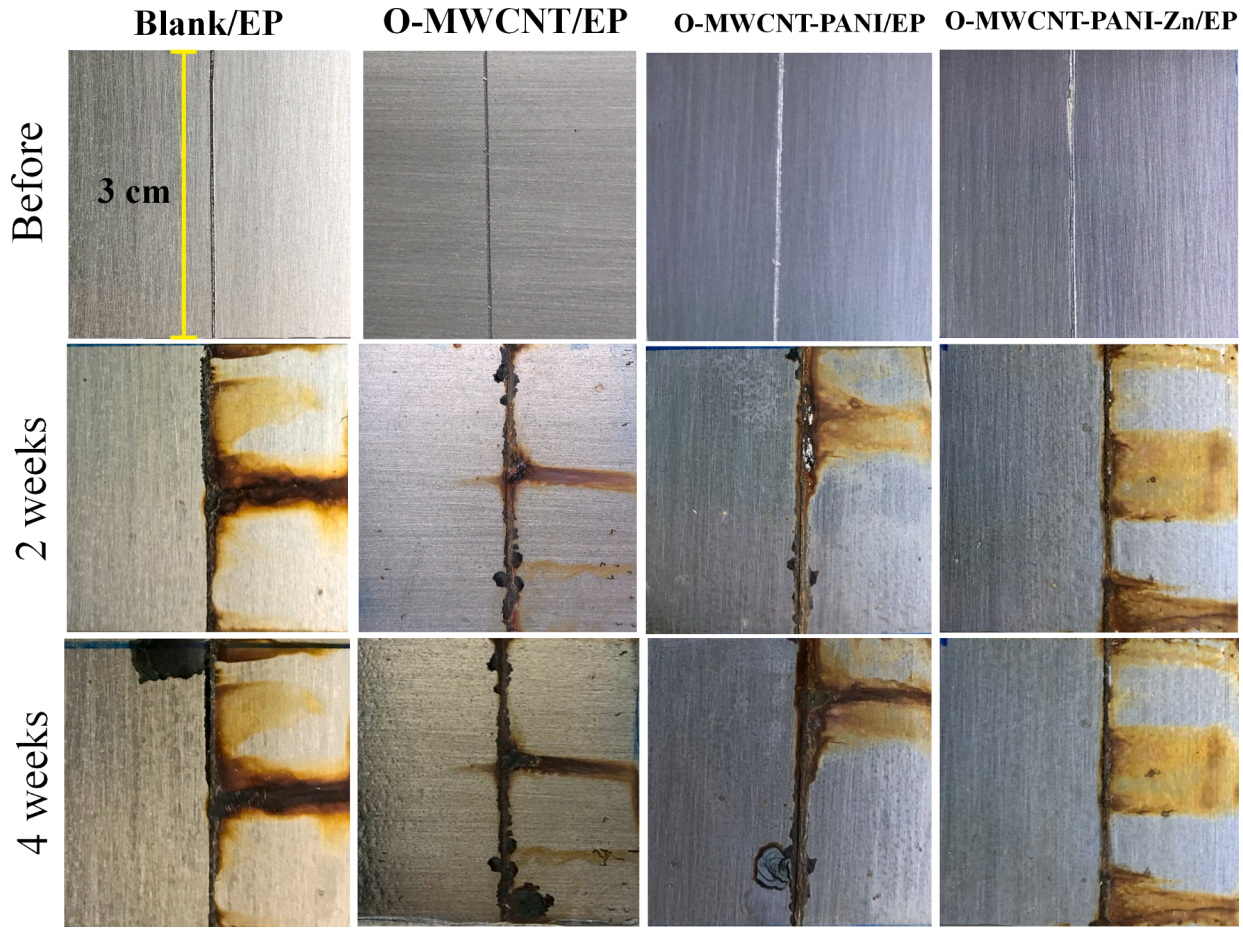

Fig. 14. Visual situation of scratched coatings exposed to salt spray for 4 weeks.

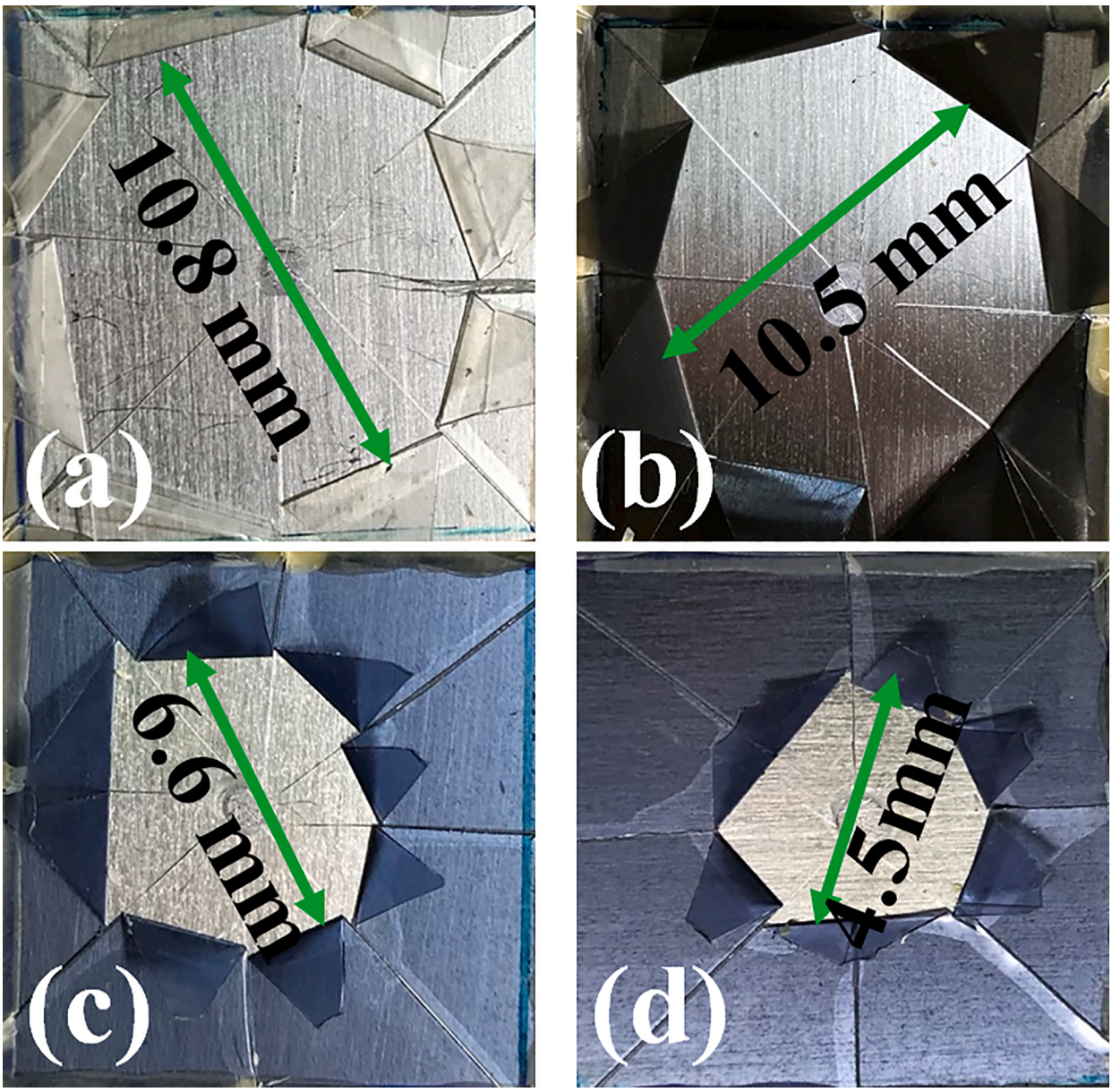

Fig. 15. Cathodic disbonding: Blank/EP (a), O-MWCNT/EP (b), O-MWCNT-PANI/EP (c), and O-MWCNT-PANI-Zn (d).

Table 9
Three different disbanding radius of Blank/EP, O-MWCNT/EP, O-MWCNT-PSNI/EP, and O-MWCNT-PANI-Zn/EP coatings.

sample	Disbonding radius repeat 1 (mm)	Disbonding radius repeat 2 (mm)	Disbonding radius repeat 3 (mm)	Average (mm)
Blank/EP	9.5	11.5	11.5	10.8
O-MWCNT/EP	10	10	11.5	10.5
O-MWCNT-PANI/EP	6	6.5	7.5	6.6
O-MWCNT-PANI-Zn/EP	4.5	5	4	4.5

Declaration of Competing Interest

The authors declare that they have no known competing financial interests or personal relationships that could have appeared to influence the work reported in this paper.

Appendix A. Supplementary data

Supplementary data to this article can be found online at https://doi.org/10.1016/j.cej.2021.128637.

References

[1] Y. Su, S. Qiu, D. Yang, S. Liu, H. Zhao, L. Wang, Q. Xue, Active anti-corrosion of epoxy coating by nitrite ions intercalated MgAl LDH, J. Hazard. Mater. 391 (2020) 122215, https://doi.org/10.1016/j.jhazmat.2020.122215.
[2] C. Chen, Y.i. He, G. Xiao, F. Zhong, Y. Xia, Y. Wu, Graphic C3N4-assisted dispersion of graphene to improve the corrosion resistance of waterborne epoxy coating, Prog. Org. Coat. 139 (2020) 105448, https://doi.org/10.1016/j.porgcoat.2019.105448.
[3] G.S. Dhole, G. Gunasekaran, R. Naik, T. Ghorpade, M. Vinjamur, Fluorescence based corrosion detecting epoxy coating, Prog. Org. Coat. 138 (2020) 105425, https://doi.org/10.1016/j.porgcoat.2019.105425.
[4] S. Brand, L. Veith, R. Baier, C. Dietrich, M.J. Schmid, T.A. Ternes, New methodical approaches for the investigation of weathered epoxy resins used for corrosion protection of steel constructions, J. Hazard. Mater. 395 (2020) 122289, https://doi.org/10.1016/j.jhazmat.2020.122289.

[5] Y. Liu, X. Zhou, S.B. Lyon, R. Emad, T. Hashimoto, A. Gholinia, G.E. Thompson, D. Graham, S.R. Gibbon, D. Francis, An organic coating pigmented with strontium aluminium polyphosphate for corrosion protection of zinc alloy coated steel, Prog. Org. Coat. 102 (2017) 29–36, https://doi.org/10.1016/j.porgcoat.2016.02.020.

[6] L.G. Ecco, M. Fedel, A. Ahniyaz, F. Deflorian, Influence of polyaniline and cerium oxide nanoparticles on the corrosion protection properties of alkyd coating, Prog. Org. Coat. 77 (2014) 2031–2038, https://doi.org/10.1016/j.porgcoat.2014.04.002.

[7] H.R. Asemani, P. Ahmadi, A.A. Sarabi, H. Eivaz Mohammadloo, Effect of zirconium conversion coating: Adhesion and anti-corrosion properties of epoxy organic coating containing zinc aluminum polyphosphate (ZAPP) pigment on carbon mild steel, Prog. Org. Coat. 94 (2016) 18–27, https://doi.org/10.1016/j.porgcoat.2016.01.015.

[8] T.T.X. Hang, N.T. Dung, T.A. Truc, N.T. Duong, B. Van Truoc, P.G. Vu, T. Hoang, D. T.M. Thanh, M.-G. Olivier, Effect of silane modified nano ZnO on UV degradation of polyurethane coatings, Prog. Org. Coat. 79 (2015) 68–74, https://doi.org/10.1016/j.porgcoat.2014.11.008.

[9] C. Wang, H. Wang, M. Li, Z. Liu, C. Lv, Y. Zhu, N. Bao, Anti-corrosion and wear resistance properties of polymer composite coatings: effect of oily functional fillers, J. Taiwan Inst. Chem. Eng. 85 (2018) 248–256, https://doi.org/10.1016/j.jtice.2018.01.031.

[10] P. Haghdadeh, M. Ghaffari, B. Ramezanzadeh, G. Bahlakeh, M.R. Saeb, The role of functionalized graphene oxide on the mechanical and anti-corrosion properties of polyurethane coating, J. Taiwan Inst. Chem. Eng. 86 (2018) 199–212, https://doi.org/10.1016/j.jtice.2018.02.009.

[11] Y.-C. Chen, A.-Y. Lu, P. Lu, X. Yang, C.-M. Jiang, M. Mariano, B. Kaehr, O. Lin, A. Taylor, I.D. Sharp, L.-J. Li, S.S. Chou, V. Tung, Structurally Deformed MoS2 for Electrochemically Stable, Thermally Resistant, and Highly Efficient Hydrogen Evolution Reaction, Adv. Mater. 29 (2017) 1703863. DOI:10.1002/adma.201703863.

[12] Y. Hao, L.A. Sani, T. Ge, Q. Fang, Phytic acid doped polyaniline containing epoxy coatings for corrosion protection of Q235 carbon steel, Appl. Surf. Sci. 419 (2017) 826–837, https://doi.org/10.1016/j.apsusc.2017.05.079.

[13] D.A. Leal, I.C. Riegel-Vidotti, M.G.S. Ferreira, C.E.B. Marino, Smart coating based on double stimuli-responsive microcapsules containing linseed oil and benzotriazole for active corrosion protection, Corros. Sci. 130 (2018) 56–63, https://doi.org/10.1016/j.corsci.2017.10.009.

[14] C. Pitakchatwong, I. Schlegel, K. Landfester, D. Crespy, S. Chirachanchai, Chitosan nanocapsules for pH-triggered dual release based on corrosion inhibitors as model study, Part. Part. Syst. Charact. 35 (2018) 1800086, https://doi.org/10.1002/ppsc.201800086.

[15] V. Shkirskiy, P. Keil, H. Hintze-Bruening, F. Leroux, P. Vialat, G. Lefèvre, K. Ogle, P. Volovitch, Factors Affecting MoO 4 2– Inhibitor Release from Zn 2 Al Based Layered Double Hydroxide and Their Implication in Protecting Hot Dip Galvanized Steel by Means of Organic Coatings, ACS Appl. Mater. Interfaces. 7 (2015) 25180–25192. DOI:10.1021/acsami.5b06702.

[16] Y. Cao, D. Zheng, X. Li, J. Lin, C. Wang, S. Dong, C. Lin, Enhanced corrosion resistance of superhydrophobic layered double hydroxide films with long-term stability on Al substrate, ACS Appl. Mater. Interfaces 10 (2018) 15150–15162, https://doi.org/10.1021/acsami.8b02280.s001.

[17] P. Vijayan P, Y.M. Hany El-Gawady, M.A.S.A. Al-Maadeed, Halloysite nanotube as multifunctional component in epoxy protective coating, Ind. Eng. Chem. Res. 55 (2016) 11186–11192, https://doi.org/10.1021/acs.iecr.6b02736.s001.

[18] D. Borisova, H. Möhwald, D.G. Shchukin, Mesoporous silica nanoparticles for active corrosion protection, ACS Nano 5 (2011) 1939–1946, https://doi.org/10.1021/nn102871v.

[19] J. Fu, T. Chen, M. Wang, N. Yang, S. Li, Y. Wang, X. Liu, Acid and alkaline dual stimuli-responsive mechanized hollow mesoporous silica nanoparticles as smart nanocontainers for intelligent anticorrosion coatings, ACS Nano 7 (2013) 11397–11408, https://doi.org/10.1021/nn4053233.

[20] S. Saadatmandi, B. Ramezanzadeh, M. Asghari, G. Bahlakeh, Graphene oxide nanoplatform surface decoration by spherical zinc-polypyrrole nanoparticles for epoxy coating properties enhancement: detailed explorations from integrated experimental and electronic-scale quantum mechanics approaches, J. Alloy. Compd. 816 (2020) 152510, https://doi.org/10.1016/j.jallcom.2019.152510.

[21] S. Pourhashem, E. Ghasemy, A. Rashidi, M.R. Vaezi, A review on application of carbon nanostructures as nanofiller in corrosion-resistant organic coatings, J. Coat. Technol. Res. 17 (2020) 19–55, https://doi.org/10.1007/s11998-019-00275-6.

[22] L. Zhai, A. Narkar, K. Ahn, Self-healing polymers with nanomaterials and nanostructures, Nano Today 30 (2020) 100826, https://doi.org/10.1016/j.nantod.2019.100826.

[23] Y. Ye, D. Yang, D. Zhang, H. Chen, H. Zhao, X. Li, L. Wang, POSS-tetraaniline modified graphene for active corrosion protection of epoxy-based organic coating, Chem. Eng. J. 383 (2020) 123160, https://doi.org/10.1016/j.cej.2019.123160.

[24] M. Rui, Y. Jiang, A. Zhu, Sub-micron calcium carbonate as a template for the preparation of dendrite-like PANI/CNT nanocomposites and its corrosion protection properties, Chem. Eng. J. 385 (2020) 123396, https://doi.org/10.1016/j.cej.2019.123396.

[25] Y. Ye, D. Zhang, T. Liu, Z. Liu, J. Pu, W. Liu, H. Zhao, X. Li, L. Wang, Superior corrosion resistance and self-healable epoxy coating pigmented with silanzied trianiline-intercalated graphene, Carbon N. Y. 142 (2019) 164–176, https://doi.org/10.1016/j.carbon.2018.10.050.

[26] W. Sun, T. Wu, L. Wang, Z. Yang, T. Zhu, C. Dong, G. Liu, The role of graphene loading on the corrosion-promotion activity of graphene/epoxy nanocomposite coatings, Compos. B Eng. 173 (2019) 106916, https://doi.org/10.1016/j.compositesb:2019.106916.

[27] X. Sheng, W. Cai, L.i. Zhong, D. Xie, X. Zhang, Synthesis of functionalized graphene/polyaniline nanocomposites with effective synergistic reinforcement on anticorrosion, Ind. Eng. Chem. Res. 55 (2016) 8576–8585, https://doi.org/10.1021/acs.iecr.6b01975.s001.

[28] Y. Tian, Y. Xie, F. Dai, H. Huang, L.i. Zhong, X. Zhang, Ammonium-grafted graphene oxide for enhanced corrosion resistance of waterborne epoxy coatings, Surf. Coat. Technol. 383 (2020) 125227, https://doi.org/10.1016/j.surfcoat.2019.125227.

[29] H. Huang, X. Huang, Y. Xie, Y. Tian, X. Jiang, X. Zhang, Fabrication of h-BN-rGO@PDA nanohybrids for composite coatings with enhanced anticorrosion performance, Prog. Org. Coat. 130 (2019) 124–131, https://doi.org/10.1016/j.porgcoat.2019.01.059.

[30] E. Pop, D. Mann, Q. Wang, K. Goodson, H. Dai, Thermal conductance of an individual single-wall carbon nanotube above room temperature, Nano Lett. 6 (2006) 96–100, https://doi.org/10.1021/nl052145f.

[31] S. Roth, V. Krstić, G.L.J.A. Rikken, Quantum transport in carbon nanotubes, Curr. Appl Phys. 2 (2002) 155–161, https://doi.org/10.1016/S1567-1739(01)00089-X.

[32] M.-F. Yu, O. Lourie, M.J. Dyer, K. Moloni, T.F. Kelly, R.S. Ruoff, Strength and Breaking Mechanism of Multiwalled Carbon Nanotubes Under Tensile Load, Science (80-.). 287 (2000) 637 LP – 640. DOI:10.1126/science.287.5453.637.

[33] M.L. Yola, T. Eren, N. Atar, Molecularly imprinted electrochemical biosensor based on Fe@Au nanoparticles involved in 2-aminoethanethiol functionalized multi-walled carbon nanotubes for sensitive determination of cefexime in human plasma, Biosens. Bioelectron. 60 (2014) 277–285, https://doi.org/10.1016/j.bios.2014.04.045.

[34] B. Ertan, T. Eren, İ. Ermiş, H. Saral, N. Atar, M.L. Yola, Sensitive analysis of simazine based on platinum nanoparticles on polyoxometalate/multi-walled carbon nanotubes, J. Colloid Interface Sci. 470 (2016) 14–21, https://doi.org/10.1016/j.jcis.2016.02.036.

[35] S. Salmanpour, A. Sadrnia, F. Karimi, N. Majani, M.L. Yola, V.K. Gupta, NiO nanoparticle decorated on single-wall carbon nanotubes and 1-butyl-4-methyl-pyridinium tetrafluoroborate for sensitive raloxifene sensor, J. Mol. Liq. 254 (2018) 255–259, https://doi.org/10.1016/j.molliq.2018.01.105.

[36] C. Onac, H. Korkmaz Alpoguz, M. Lutfi Yola, A. Kaya, Transport of melamine by a new generation of nano-material membranes containing carbon nanotubes and determination with surface plasmon resonance, Innov. Food Sci. Emerg. Technol. 45 (2018) 467–470, https://doi.org/10.1016/j.ifset.2017.07.003.

[37] M.L. Yola, N. Atar, A novel voltammetric sensor based on gold nanoparticles involved in p-aminothiophenol functionalized multi-walled carbon nanotubes: application to the simultaneous determination of quercetin and rutin, Electrochim. Acta 119 (2014) 24–31, https://doi.org/10.1016/j.electacta.2013.12.028.

[38] K. Yang, M. Gu, Y. Guo, X. Pan, G. Mu, Effects of carbon nanotube functionalization on the mechanical and thermal properties of epoxy composites, Carbon 47 (2009) 1723–1737, https://doi.org/10.1016/j.carbon.2009.02.029.

[39] K. Tao, S. Yang, J.C. Grunlan, Y.-S. Kim, B. Dang, Y. Deng, R.L. Thomas, B. L. Wilson, X. Wei, Effects of carbon nanotube fillers on the curing processes of epoxy resin-based composites, J. Appl. Polym. Sci. 102 (2006) 5248–5254, https://doi.org/10.1002/app.24773.

[40] L.-C. Tang, H. Zhang, J.-H. Han, X.-P. Wu, Z. Zhang, Fracture mechanisms of epoxy filled with ozone functionalized multi-wall carbon nanotubes, Compos. Sci. Technol. 72 (2011) 7–13, https://doi.org/10.1016/j.compscitech.2011.07.016.

[41] M.R. Mansor, S.H.S.M. Fadzullah, N.A.B. Masripan, G. Omar, M.Z. Akop, Comparison Between Functionalized Graphene and Carbon Nanotubes: Effect of Morphology and Surface Group on Mechanical, Electrical, and Thermal Properties of Nanocomposites, Elsevier Inc., 2018. DOI:10.1016/B978-0-12-814548-7.00009-X.

[42] S. Park, M. Shon, Effects of multi-walled carbon nano tubes on corrosion protection of zinc rich epoxy resin coating, J. Ind. Eng. Chem. 21 (2015) 1258–1264, https://doi.org/10.1016/j.jiec.2014.05.042.

[43] R. Asmatulu, G.A. Mahmud, C. Hille, H.E. Misak, Effects of UV degradation on surface hydrophobicity, crack, and thickness of MWCNT-based nanocomposite coatings, Prog. Org. Coat. 72 (2011) 553–561, https://doi.org/10.1016/j.porgcoat.2011.06.015.

[44] N.W. Khun, B.C.R. Troconis, G.S. Frankel, Effects of carbon nanotube content on adhesion strength and wear and corrosion resistance of epoxy composite coatings on AA2024-T3, Prog. Org. Coat. 77 (2014) 72–80, https://doi.org/10.1016/j.porgcoat.2013.08.003.

[45] H. Jeon, J. Park, M. Shon, Corrosion protection by epoxy coating containing multi-walled carbon nanotubes, J. Ind. Eng. Chem. 19 (2013) 849–853, https://doi.org/10.1016/j.jiec.2012.10.030.

[46] H. Yu, Y. Jin, F. Peng, H. Wang, Kinetically controlled side-wall functionalization of carbon nanotubes by nitric acid oxidation, J. Phys. Chem. C (ACS Publications) J. Phys. 112 (2008) 6758–6763, https://doi.org/10.1021/Jp711975a.

[47] M. Bayazit, K. Coleman, … -Walled Carbon Nanotubes Following the 1, 3-Dipolar Cycloaddition of Pyridinium …, J. Am. Chem. …. (2009) 10670–10676. http://www.ncbi.nlm.nih.gov/pubmed/19569688%5Cnfile:///Users/Tim/Documents/Papers2/Articles/2009/Bayazit/Journal of the American Chemical …/Journal of the American Chemical … 2009 Bayazit… -Walled Carbon Nanotubes Following.pdf%5Cnpape.

[48] Y. Gao, I. Kyratzis, Covalent immobilization of proteins on carbon nanotubes using the, Bioconjug. Chem. 19 (2008) 1945–1950.

[49] A.A. Koval'chuk, V.G. Shevchenko, A.N. Shchegolikhin, P.M. Nedorezova, A. N. Klyamkina, A.M. Aladyshev, Effect of carbon nanotube functionalization on the structural and mechanical properties of polypropylene/MWCNT composites, Macromolecules 41 (2008) 7536–7542, https://doi.org/10.1021/ma801599q.

[50] J. Gao, B. Zhao, M.E. Itkis, E. Bekyarova, H. Hu, V. Kranak, A. Yu, R.C. Haddon, 02 J.Am.Chem.Soc.2006,128,7492-7496.pdf, (2006) 7492–7496.
[51] I.-Y. Jeon, H.-J. Lee, Y.S. Choi, L.-S. Tan, J.-B. Baek, Semimetallic transport in nanocomposites derived from grafting of linear and hyperbranched poly (phenylene sulfide)s onto the surface of functionalized multi-walled carbon nanotubes, Macromolecules 41 (2008) 7423–7432, https://doi.org/10.1021/ma801259b.
[52] B. Ramezanzadeh, M.H. Mohamadzadeh Moghadam, N. Shohani, M. Mahdavian, Effects of highly crystalline and conductive polyaniline/graphene oxide composites on the corrosion protection performance of a zinc-rich epoxy coating, Chem. Eng. J. 320 (2017) 363–375, https://doi.org/10.1016/j.cej.2017.03.061.
[53] F. Fekri, M. Shahidi Zandi, M.M. Foroughi, Polypyrrole coatings for corrosion protection of Al alloy2024: influence of electrodeposition methods, solvents, and ZnO nanoparticle concentrations, Iran Polym. J. 28 (2019) 577–585, https://doi.org/10.1007/s13726-019-00726-2.
[54] S. Qiu, W. Li, W. Zheng, H. Zhao, L. Wang, Synergistic effect of polypyrrole-intercalated graphene for enhanced corrosion protection of aqueous coating in 3.5% NaCl solution, ACS Appl. Mater. Interfaces 9 (2017) 34294–34304, https://doi.org/10.1021/acsami.7b08325.s001.
[55] A. Habibiyan, B. Ramezanzadeh, M. Mahdavian, M. Kasaeian, Facile size and chemistry-controlled synthesis of mussel-inspired bio-polymers based on polydopamine nanospheres: application as eco-friendly corrosion inhibitors for mild steel against aqueous acidic solution, J. Mol. Liq. 298 (2020) 111974, https://doi.org/10.1016/j.molliq.2019.111974.
[56] M.-S. Hong, Y. Park, T. Kim, K. Kim, J.-G. Kim, Polydopamine/carbon nanotube nanocomposite coating for corrosion resistance, J. Materiomics 6 (2020) 158–166, https://doi.org/10.1016/j.jmat.2020.01.004.
[57] G. Cai, J. Hou, Z. Dong, Polydopamine-wrapped carbon nanotubes to improve the corrosion barrier of polyurethane, (2018) 23727–23741. DOI:10.1039/c8ra03267j.
[58] M. Izadi, T. Shahrabi, B. Ramezanzadeh, Synthesis and characterization of an advanced layer-by-layer assembled Fe 3 O 4 /polyaniline nanoreservoir filled with Nettle extract as a green corrosion protective system, J. Ind. Eng. Chem. 57 (2018) 263–274, https://doi.org/10.1016/j.jiec.2017.08.032.
[59] E. Armelin, R. Pla, F. Liesa, X. Ramis, José.I. Iribarren, C. Alemán, Corrosion protection with polyaniline and polypyrrole as anticorrosive additives for epoxy paint, Corros. Sci. 50 (2008) 721–728, https://doi.org/10.1016/j.corsci.2007.10.006.
[60] B. Ramezanzadeh, P. Kardar, G. Bahlakeh, Y. Hayatgheib, M. Mahdavian, Fabrication of a highly tunable graphene oxide composite through layer-by-layer assembly of highly crystalline polyaniline nanofibers and green corrosion inhibitors: complementary experimental and first-principles quantum-mechanics modeling approaches, J. Phys. Chem. C 121 (2017) 20433–20450, https://doi.org/10.1021/acs.jpcc.7b04323.s001.
[61] N.N. Taheri, B. Ramezanzadeh, M. Mahdavian, Application of layer-by-layer assembled graphene oxide nanosheets/polyaniline/zinc cations for construction of an effective epoxy coating anti-corrosion system, J. Alloy. Compd. 800 (2019) 532–549, https://doi.org/10.1016/j.jallcom.2019.06.103.
[62] B. Ramezanzadeh, G. Bahlakeh, M. Ramezanzadeh, Polyaniline-cerium oxide (PAni-CeO 2) coated graphene oxide for enhancement of epoxy coating corrosion protection performance on mild steel, Corros. Sci. 137 (2018) 111–126, https://doi.org/10.1016/j.corsci.2018.03.038.
[63] Y. Hayatgheib, B. Ramezanzadeh, P. Kardar, M. Mahdavian, A comparative study on fabrication of a highly effective corrosion protective system based on graphene oxide-polyaniline nanofibers/epoxy composite, Corros. Sci. 133 (2018) 358–373, https://doi.org/10.1016/j.corsci.2018.01.046.
[64] S. Amrollahi, B. Ramezanzadeh, H. Yari, M. Ramezanzadeh, M. Mahdavian, Synthesis of polyaniline-modified graphene oxide for obtaining a high performance epoxy nanocomposite film with excellent UV blocking/anti-oxidant/ anti-corrosion capabilities, Compos. B Eng. 173 (2019) 106804, https://doi.org/10.1016/j.compositesb:2019.05.015.
[65] S. Akbarzadeh, M. Ramezanzadeh, B. Ramezanzadeh, M. Mahdavian, R. Naderi, Fabrication of highly effective polyaniline grafted carbon nanotubes to induce active protective functioning in a silane coating, Ind. Eng. Chem. Res. 58 (2019) 20309–20322, https://doi.org/10.1021/acs.iecr.9b04217.
[66] M.-C. Bernard, A. Hugot-LeGoff, S. Joiret, N.N. Dinh, N.N. Toan, Polyaniline layer for iron protection in sulfate medium, Synth. Met. 102 (1999) 1383–1384, https://doi.org/10.1016/S0379-6779(98)01001-7.
[67] R. Racicot, R. Brown, S.C. Yang, Corrosion protection of aluminum alloys by double-strand polyaniline, Synth. Met. 85 (1997) 1263–1264, https://doi.org/10.1016/S0379-6779(97)80232-9.
[68] M. Fahlman, S. Jasty, A.J. Epstein, Corrosion protection of iron/steel by emeraldine base polyaniline: an X-ray photoelectron spectroscopy study, Synth. Met. 85 (1997) 1323–1326, https://doi.org/10.1016/S0379-6779(97)80256-1.
[69] J.-C. Lacroix, J.-L. Camalet, S. Aeiyach, K.I. Chane-Ching, J. Petitjean, E. Chauveau, P.-C. Lacaze, Aniline electropolymerization on mild steel and zinc in a two-step process, J. Electroanal. Chem. 481 (2000) 76–81, https://doi.org/10.1016/S0022-0728(99)00490-8.
[70] Z. Tian, H. Yu, L. Wang, M. Saleem, F. Ren, P. Ren, RSC Advances nanostructures and their applications in anticorrosive coatings, (2014) 28195–28208. DOI: 10.1039/c4ra03146f.
[71] D. Song, Z. Yin, F. Liu, H. Wan, J. Gao, D. Zhang, X. Li, Effect of carbon nanotubes on the corrosion resistance of water-borne acrylic coatings, Prog. Org. Coat. 110 (2017) 182–186, https://doi.org/10.1016/j.porgcoat.2017.04.043.
[72] M.A. Deyab, Effect of carbon nano-tubes on the corrosion resistance of alkyd coating immersed in sodium chloride solution, Prog. Org. Coat. 85 (2015) 146–150, https://doi.org/10.1016/j.porgcoat.2015.04.003.
[73] N.N. Taheri, B. Ramezanzadeh, M. Mahdavian, G. Bahlakeh, In-situ synthesis of Zn doped polyaniline on graphene oxide for inhibition of mild steel corrosion in 3.5 wt.% chloride solution, J. Ind. Eng. Chem. 63 (2018) 322–339, https://doi.org/10.1016/j.jiec.2018.02.033.
[74] A. Dehghani, G. Bahlakeh, B. Ramezanzadeh, Designing a novel targeted-release nano-container based on the silanized graphene oxide decorated with cerium acetylacetonate loaded beta-cyclodextrin (β-CD-CeA-MGO) for epoxy anti-corrosion coating, Chem. Eng. J. 400 (2020) 125860, https://doi.org/10.1016/j.cej.2020.125860.
[75] Z. Dong, A. Poursaee, Corrosion behavior of coupled active and passive reinforcing steels in simulated concrete pore solution, Constr. Build. Mater. 240 (2020) 117955, https://doi.org/10.1016/j.conbuildmat.2019.117955.
[76] H. Elmsellem, T. Harit, A. Aouniti, F. Malek, A. Riahi, A. Chetouani, B. Hammouti, Adsorption properties and inhibition of mild steel corrosion in 1 M HCl solution by some bipyrazolic derivatives: experimental and theoretical investigations, Prot. Met. Phys. Chem. Surf. 51 (2015) 873–884, https://doi.org/10.1134/S207020511505007X.
[77] M. Tabatabaei majd, G. Bahlakeh, A. Dehghani, B. Ramezanzadeh, M. Ramezanzadeh, Combined molecular simulation, DFT computation and electrochemical studies of the mild steel corrosion protection against NaCl solution using aqueous Eucalyptus leaves extract molecules linked with zinc ions, J. Mol. Liq. 294 (2019) 111550, https://doi.org/10.1016/j.molliq.2019.111550.
[78] S. Akbarzadeh, B. Ramezanzadeh, G. Bahlakeh, M. Ramezanzadeh, Molecular/electronic/atomic-level simulation and experimental exploration of the corrosion inhibiting molecules attraction at the steel/chloride-containing solution interface, J. Mol. Liq. 296 (2019) 111809, https://doi.org/10.1016/j.molliq.2019.111809.
[79] M. Karamać, Chelation of Cu(II), Zn(II), and Fe(II) by Tannin Constituents of Selected Edible Nuts, Int. J. Mol. Sci. 10 (2009) 5485–5497. DOI:10.3390/ijms10125485.
[80] K. Woo, H.J. Lee, J.-P. Ahn, Y.S. Park, Sol–gel mediated synthesis of Fe2O3 nanorods, Adv. Mater. 15 (2003) 1761–1764, https://doi.org/10.1002/adma.200305561.
[81] J. Wang, L. Li, C.L. Wong, L. Sun, Z. Shen, S. Madhavi, Controlled synthesis of α-FeOOH nanorods and their transformation to mesoporous α-Fe2O3, Fe3O4@C nanorods as anodes for lithium ion batteries, RSC Adv. 3 (2013) 15316, https://doi.org/10.1039/c3ra41886c.
[82] K. Hedenstedt, J. Bäckström, E. Ahlberg, In-Situ Raman spectroscopy of α- and γ-FeOOH during cathodic load, J. Electrochem. Soc. 164 (2017) H621–H627, https://doi.org/10.1149/2.0731709jes.
[83] C. Rémazeilles, P. Refait, On the formation of β-FeOOH (akaganéite) in chloride-containing environments, Corros. Sci. 49 (2007) 844–857, https://doi.org/10.1016/j.corsci.2006.06.003.
[84] H. Xiong, F. Qi, N. Zhao, H. Yuan, P. Wan, B. Liao, X. Ouyang, Effect of organically modified sepiolite as inorganic nanofiller on the anti-corrosion resistance of epoxy coating, Mater. Lett. 260 (2020) 126941, https://doi.org/10.1016/j.matlet.2019.126941.
[85] Y.-T. Lin, T.-M. Don, C.-J. Wong, F.-C. Meng, Y.-J. Lin, S.-Y. Lee, C.-F. Lee, W.-Y. Chiu, Improvement of mechanical properties and anticorrosion performance of epoxy coatings by the introduction of polyaniline/graphene composite, Surf. Coat. Technol. 374 (2019) 1128–1138, https://doi.org/10.1016/j.surfcoat.2018.01.050.
[86] C.-H. Chang, T.-C. Huang, C.-W. Peng, T.-C. Yeh, H.-I. Lu, W.-I. Hung, C.-J. Weng, T.-I. Yang, J.-M. Yeh, Novel anticorrosion coatings prepared from polyaniline/graphene composites, Carbon 50 (2012) 5044–5051, https://doi.org/10.1016/j.carbon.2012.06.043.
[87] A.A. Javidparvar, R. Naderi, B. Ramezanzadeh, L-cysteine reduced/functionalized graphene oxide application as a smart/control release nanocarrier of sustainable cerium ions for epoxy coating anti-corrosion properties improvement, J. Hazard. Mater. 389 (2020) 122135, https://doi.org/10.1016/j.jhazmat.2020.122135.
[88] A.A. Javidparvar, R. Naderi, B. Ramezanzadeh, Designing a potent anti-corrosion system based on graphene oxide nanosheets non-covalently modified with cerium/benzimidazole for selective delivery of corrosion inhibitors on steel in NaCl media, J. Mol. Liq. 284 (2019) 415–430, https://doi.org/10.1016/j.molliq.2019.04.028.
[89] A. Habibiyan, B. Ramezanzadeh, M. Mahdavian, G. Bahlakeh, M. Kasaeian, Rational assembly of mussel-inspired polydopamine (PDA)-Zn (II) complex nanospheres on graphene oxide framework tailored for robust self-healing anti-corrosion coatings application, Chem. Eng. J. 391 (2020) 123630, https://doi.org/10.1016/j.cej.2019.123630.